

# Star formation activity and gas stripping in the Cluster Projected Phase-Space (CPPS)

Jonathan D. Hernández-Fernández<sup>1</sup>, C. P. Haines<sup>2</sup>, A. Diaferio<sup>3,4</sup>, J. Iglesias-Páramo<sup>5,6</sup>,  
C. Mendes de Oliveira<sup>1</sup> and J. M. Vilchez<sup>5</sup>

## ABSTRACT

This work is focused on the study of the distribution in the CPPS of passive(ly-evolving) and star-forming galaxy populations and also, the intense and quiescent star-forming populations for a set of nine nearby  $z < 0.05$  galaxy clusters. Furthermore, we compare the CPPS distribution of the passive galaxy population with the accreted halo population of a set of 28 simulated clusters and the star-forming population with the non-accreted population. We consider various cluster accretion epochs and accretion radii where it is assumed that star formation in galaxies becomes quenched, in order to segregate the accreted population from the non-accreted population. Just applying this segregation in simulations, we get a qualitative agreement between the CPPS distributions of the passive and the accreted populations and also between the star-forming and the non-accreted populations. The uncertainty in cluster centering strongly affects the pronounced cuspy profiles of the projected density and also, it can explain the main difference (i.e. inner slope) between the CPPS distribution of passive and accreted populations. The CPPS density of star-forming galaxies and the intensity of ram-pressure stripping present an opposite trend throughout the CPPS. This implies that ram-pressure stripping significantly contributes to modulate the observed CPPS distribution of star-forming galaxies in cluster virial regions and their surroundings. The significant fraction of star-forming galaxies at the projected center of clusters are mainly those galaxies with low l-o-s velocities and they can be mainly identified as those galaxies with a remaining star formation activity (quiescent star-forming galaxies) inside the physical virial region or, in a lower degree, as galaxy interlopers i.e. outside the physical virial region. This article also includes a test of the effects caused by the Sloan fibre collision on the completeness of the Main Galaxy Sample as a function of clustercentric radius.

*Subject headings:* galaxies: clusters: general, galaxies: evolution, galaxies: star formation, ultraviolet: galaxies

---

<sup>1</sup>Departamento de Astronomia, Instituto de Astronomia, Geofísica e Ciências Atmosféricas da Universidade de São Paulo, Rua do Matão 1226, Cidade Universitária, 05508-090, São Paulo, Brazil; jonatan.fernandez@iag.usp.br

<sup>2</sup>Observatorio Astronómico Cerro Calán, Departamento de Astronomía, Universidad de Chile, Casilla 36-D Santiago, Chile

<sup>3</sup>Dipartimento di Fisica, Università di Torino, V. Pietro Giuria 1, 10125 Torino, Italy

<sup>4</sup>Istituto Nazionale di Fisica Nucleare (INFN), Sezione di Torino, V. Pietro Giuria 1, 10125 Torino, Italy

<sup>5</sup>Instituto de Astrofísica de Andalucía, Glorieta de la Astronomía s/n, 18008 Granada

<sup>6</sup>Centro Astronómico Hispano Alemán C/ Jesús Durbán

## 1. Introduction

Galaxies, especially in clusters, are under the influence of a number of environmental processes producing a strong impact on their stellar and gaseous components and their global properties as morphology, star formation activity, etc. The specific contribution of each one of these processes, which can operate alone or simultaneously, to the modulation of galaxy properties is an issue which is not totally clarified so far. Several authors (e.g. Dickens & Moss

---

Remón, 2-2 04004 Almería

1976; Colless & Dunn 1996; Mohr et al. 1996; Biviano et al. 1997; Carlberg et al. 1997; Fisher et al. 1998; de Theije & Katgert 1999; Biviano et al. 2002; Diaferio et al. 2001) have pointed out that the combined study of the spatial and kinematic variables of galaxy distributions in clusters as a function of galaxy properties and galaxy populations, is key to shedding light on how the cluster galaxy population is formed. The most appropriate space which combines these variables is the Cluster Projected Phase-Space (CPPS). This space is defined by the cluster-centric projected radius  $R_P$  normalized by the virial radius  $r_{200}$ ,  $\tilde{r}=R_P/r_{200}$  and the cluster-frame line-of-sight velocity  $c\Delta z/(1+z_c)$  normalized by the rest-frame cluster velocity dispersion  $\sigma_c$ ,  $\tilde{s}=(c\Delta z/(1+z_c))/\sigma_c$ .

A precise estimation of the impact of environmental processes along the history of a galaxy orbiting its parent cluster is rather difficult due to the nature of galaxy clusters. First of all, the observed velocity dispersions of  $\sim 1000 \text{ km s}^{-1}$  for rich galaxy clusters imply that we normally cannot measure the l-o-s distance to a given spectroscopic cluster member to an accuracy better than  $\sim 15 \text{ Mpc}$ . Thus, we cannot identify whether it is in the cluster core, in the outskirts, or even whether it has ever felt any environmental influence of the cluster. Furthermore, clusters contain a backsplash galaxy population which is composed of those galaxies which, after reaching the pericenter of their orbits and suffering the environmental effects of virial regions, currently show a position well outside the virial region (Gill et al. 2005; Sato & Martin 2006; Pimbblet 2011; Mahajan et al. 2011; Oman et al. 2013). This population has been invoked to explain the presence of HI-stripped galaxies out to large radii outside the central regions of clusters (Solanes et al. 2001). In addition, a pre-processing scenario (Fujita 2004) is proposed for those galaxies mainly affected by tidal interactions within the frame of galaxy groups or filaments feeding galaxy clusters but outside the virial region (Porter et al. 2008; Bahé et al. 2013; Dressler et al. 2013; Lopes et al. 2013), with the case of the Blue Infalling Group (Iglesias-Paramo et al. 2002; Cortese et al. 2006) as the prototype.

Nevertheless, some properties of galaxy population as star-forming activity, morphology or

galaxy luminosity show a significant degree of segregation as a function of the environmental conditions. These environmental conditions are spatial conditions e.g. cluster-centric radius, volume density of galaxies, or kinematical conditions such as the velocity distribution of the galaxy system or the type of orbits around the cluster. Here, we outline a few of these trends. The  $\text{H}\alpha$  emission as a tracer of the very recent star-formation activity presents a trend in fraction of star-forming galaxies and the intensity of star-formation activity depending on environmental conditions as the clustercentric radius (e.g. Lewis et al. 2002; Balogh et al. 2004; Koopmann & Kenney 2004; Rines et al. 2005; Hwang & Lee 2008). There are a number of works which found that late-type galaxies in clusters have statistically significant higher velocity dispersion than that shown by early-type galaxies (e.g. Sodre et al. 1989; Biviano & Katgert 2004; Goto 2005a). Regarding the galaxy luminosity, the brightest cluster galaxy (or the set of brightest galaxies) shows a systematic lower velocity departure from the cluster average velocity than the rest of the galaxies (e.g. Adami et al. 1998a; Goto 2005a; Hwang & Lee 2008) or in some cases well away from the mean cluster velocity (Pimbblet et al. 2006). Recently, Haines et al. (2012) have presented a study of the CPPS distribution of X-ray active galactic nuclei (AGN) for a representative sample of massive clusters at intermediate redshifts, providing evidence that X-ray AGNs found in massive clusters are an infalling population. Assuming three different categories of orbits (radial, circular and isotropic) depending on the budget between the radial component and the tangential component of the galaxy velocity vector; some authors find a distinct orbital behaviour for different (morphological and/or spectral) galaxy populations (e.g. Ramirez & de Souza 1998; Biviano & Katgert 2004; Adami et al. 1998c). In contrast, other works claim there is no significant difference between orbital distribution for different cluster galaxy populations (e.g. Rines et al. 2003; van der Marel et al. 2000; Goto 2005a).

Assuming the CPPS contains two prominent observables (clustercentric radius and cluster-frame line-of-sight velocity) which strongly determine the intensity of the different environmental processes, it is crucial to the study the distribution

of the different galaxy populations in this phase-space, in order to assess the specific influence of each process in the build up of each galaxy population. In this article, we focus on the study of the observed distributions of galaxies in the CPPS depending on their level of star-formation activity. We will deal with two galaxy dichotomies; passive vs. star-forming galaxies and quiescent vs. intense star-forming galaxies. In order to divide cluster galaxies between passive and star-forming galaxies, we take advantage of vacuum ultraviolet (UV) data from GALEX (Galaxy Evolution Explorer) (Morrissey et al. 2005; Martin et al. 2005). The vacuum UV stellar emission is a robust tracer of the recent star formation because it comes from the more short-lived stars  $\tau < 10^8$  yr (Kennicutt 1998; Kauffmann et al. 2007; Martin et al. 2005).

The remainder of this paper is organised as follows. In section 2 we describe the set of galaxy clusters studied in this work and the improved estimation of their cluster properties. In section 3, we present the results on the segregation of passive and star-forming galaxies in the CPPS in subsection 3.1 and the expected distribution of galaxy halos in the CPPS depending on the accretion epoch and the accretion radius i.e. the time and the radius where it is assumed the star formation in a galaxy starts to be quenched, dividing them between formerly accreted and non-accreted halos in subsection 3.2. The motivation of Section 4 is establishing links between the accretion history of cluster galaxies and their star-formation mode, passive or star-forming. Assuming the global shape of a CPPS distribution comes from the combination of the velocity distribution and the radial profile of the projected density, we discuss the comparison of these two observables between the halo populations and the galaxy populations in detail in this section. In subsection 4.1, we discuss about the effect of uncertainties of cluster centering in the derivation of the density profile and the effect of uncertainties of cluster average redshift in the derivation of the velocity distribution. In subsection 4.2 we assess and describe the influence of the ram-pressure on the modulation of the star-formation activity in the framework of the CPPS and in subsection 4.3 we probe and describe the distribution of star-forming galaxies split by their intensity of star-formation activity. In section 5 we summarize the main results and conclu-

sions of this work. In Appendix, we compute the effect of incompleteness of the Main Galaxy Sample (Strauss et al. 2002) as a function of cluster-centric radius. Throughout the paper, all physical magnitudes are computed assuming a cosmological model characterized by the following parameters:  $h=0.7$ ,  $\Omega_m=0.3$  and  $\Omega_\Lambda=0.7$ .

## 2. The set of galaxy clusters

The set of galaxy clusters under study in this work is taken from the sample of cluster galaxies extensively described in Hernández-Fernández et al. (2012a, hereafter Paper I). This sample consists of a total of more than 5000 galaxies distributed in 16 nearby clusters ( $z < 0.05$ ) showing a rich variety in their properties, from poor to rich clusters. The galaxy sample spans an  $r'$ -band luminosity range corresponding to  $-23 \lesssim M_{r'} \lesssim -18$ . The faint limit in this magnitude range corresponds approximately to the classical luminosity boundary between giant and dwarf galaxies  $M_B \sim -18$ . The selection of this sample was constrained by the condition that it be covered by the Data Release 6 of the Main Galaxy Sample (MGS) of SDSS (Adelman-McCarthy et al. 2008) and the AIS (All Imaging Survey) of GALEX mission (Martin et al. 2005). We restrict the UV data to the AIS in order to keep a homogeneous completeness in the UV bands for the galaxy sample. The completeness limit in AB-magnitude corrected for Galactic extinction of  $NUV \sim 22.5$  for the SDSS-GALEX matched catalog (Bianchi et al. 2007) and the completeness limit of the SDSS MGS in the  $r'$ -band composite-model magnitude  $r'=17.56$  allow us to robustly identify and segregate star-forming galaxies from passive galaxies down to the MGS SDSS magnitude limit (see Figure 4 of Hernández-Fernández et al. 2012b).

Given that this work is focused on the study of the CPPS, we require an accurate estimation of the cluster center, the average redshift and the velocity dispersion of each cluster. For this purpose, we rely on the caustic method (Diaferio & Geller 1997; Diaferio 1999). The caustic method, originally proposed by Diaferio & Geller (1997), is an approach which provides the mass profile and the profile of the escape velocity along the line of sight  $\langle v_{\text{esc}}^2 \rangle_{l.o.s}$  out to cluster regions well beyond  $r_{200}$ , using only the galaxy celestial coordinates and

redshifts, and without assuming dynamical equilibrium for the cluster (Diaferio 1999). It is important to say that the caustic method includes the hierarchical clustering method (Serna & Gerbal 1996; Diaferio 1999) for the cluster center determination which is unbiased with respect to the center of mass of the cluster. We note that the velocity dispersion retrieved from a set of simulated clusters through the caustic method in Serra et al. (2011) is in good agreement with the *true* velocity dispersion, defined as the line-of-sight velocity dispersion of the particles within a sphere of radius  $3r_{200}$  in real space. In fact, the caustic velocity dispersion was found to be within 5% of the true value for the 50% of the cluster set and within 30% of the true value for the 95% of the cluster set. Serra et al. (2011) also show that a few tens of redshifts per squared comoving megaparsec within the cluster, are enough to derive a reasonably accurate estimate of the escape velocity profile out to around  $4r_{200}$ . Regarding the cluster centering, the caustic method provides cluster centers which differs, on average, approximately 150 kpc from the X-ray centroids for a X-ray cluster catalogue of 72 clusters in Rines & Diaferio (2006). We apply the caustic method to a set of nine massive ( $\sigma_c \gtrsim 500 \text{ km s}^{-1}$ ) clusters; the resulting cluster centers, average redshifts, rest-frame velocity dispersions and other derived cluster properties are reported in Table 1. In this cluster set, we include the seven massive clusters ( $\sigma_c > 500 \text{ km s}^{-1}$ ) from the original sample and also ABELL 2197 and WBL 518. We include just massive clusters to avoid the poor statistics and the less accurate cluster properties (cluster center, velocity dispersion, etc) provided by poor galaxy groups. The two clusters explicitly outlined are included in the galaxy sample described in Hernández-Fernández et al. (2012a) but initially they were not selected as ‘central’ clusters in the original sample (see section 3 in Hernández-Fernández et al. 2012b).

The comparison of the *caustic* velocity dispersions with respect to the values of velocity dispersion computed through the Poggianti et al. (2006)’s procedure (see Paper I) produces an agreement within  $\Delta\sigma_c \lesssim 150 \text{ km s}^{-1}$  among the seven clusters in common with the original sample and of the same order of magnitude of the uncertainty of the cluster velocity dispersion  $\delta\sigma_c \sim 50-$

Table 1: **Caustic properties of the observed cluster set.**

Cluster	$\alpha_c$ deg	$\delta_c$ deg	$z_c$
(1)	(2)	(3)	(4)
ABELL 671	127.133	30.415	0.04952
ABELL 1185	167.654	28.691	0.03325
ABELL 1213	169.125	29.266	0.04671
WBL 514	218.518	3.783	0.02864
WBL 518	220.170	3.459	0.02717
UGC1 393	244.447	35.035	0.03160
B2(*)	245.742	37.943	0.03077
ABELL 2199	247.144	39.552	0.03035
ABELL 2197E	247.483	40.650	0.03024

$z_{GA}$	$\sigma_c$ km s <sup>-1</sup>	$r_{200}$ Mpc	$M_{200}$ $10^{14} M_\odot$
(5)	(6)	(7)	(8)
0.05013	715.16	1.727	6.127
0.03476	1165.24	2.834	26.694
0.04813	682.02	1.649	5.319
0.03069	492.76	1.201	2.023
0.02923	505.55	1.233	2.186
0.03314	505.63	1.231	2.183
0.03225	508.74	1.239	2.224
0.03180	742.21	1.808	6.908
0.03168	692.85	1.688	5.620

(1) NED Object Name of the cluster. The complete NED name of B2(\*) is B2 1621+38:[MLO2002] CLUSTER, (2) and (3) Celestial coordinates of cluster center, (4) average redshift and (5) redshift corrected from nearby attractors computed with Moustakas IDL procedure *mould\_distance.pro* from <http://code.google.com/p/idl-moustakas/> following Mould et al. (2000) (6) rest-frame cluster velocity dispersion computed through the caustic method, (7)  $r_{200}$  and (8)  $M_{200}$  are, respectively, the virial radius and the virial mass computed following Finn et al. (2005) using the  $\sigma_c$  as input.

100 km s<sup>-1</sup>, except for the case of ABELL 1185, the more massive cluster, with a difference of  $\Delta\sigma_c \sim 375 \text{ km s}^{-1}$ . In the case of the offsets in ce-

lestial coordinates of cluster centers, they are less than  $\Delta\theta\sim 3.15$  arcmin between clusters in common with the original sample. This offset corresponds to  $\sim 115$  kpc in physical distance at  $z=0.03$ . We stress that the *caustic* cluster center as a more robust estimation than the values reported by NED insofar it is unbiased with respect to the center of mass of the cluster.

### 3. Results: Distribution of galaxies in the CPPS

#### 3.1. Passive and star-forming cluster galaxies in the CPPS

In order to separate the star-forming galaxies from the passively-evolving galaxies, we apply the UV-optical color cut proposed for the (NUV- $r'$ ) vs. ( $u'-r'$ ) color-color diagram in Paper I. Specifically, we assume a galaxy is a star-forming galaxy if it fulfils one of the following conditions:

$$u'-r' < 2.175 \text{ and } \text{NUV}-r' < -4.9$$

$$u'-r' > 2.175 \text{ and } \text{NUV}-r' < -2(u'-r') + 9.25 \text{ or}$$

$u'-r' < 2.22$  and there is no GALEX counterpart for this specific galaxy.

Otherwise, we classify the galaxy as a passive galaxy.

The integrated NUV- $r'$  colour is enough to provide a robust separation of passive and star-forming galaxies (Salim et al. 2005; Kauffmann et al. 2007; Martin et al. 2007) with a scarce presence (less than  $\sim 10$  per cent) of H $\alpha$  emission-line galaxies in the UV-optical red sequence (Haines et al. 2008). Also, the combined UV-optical color-color diagrams are suitable to detect galaxies with truncated star formation histories (Kaviraj et al. 2007). Furthermore, the integrated ultraviolet and optical colors present the advantage with respect to the fiber spectra of not suffering from the aperture bias effect (e.g. Kewley et al. 2005). This effect easily produces the miss-classification of those early-spiral galaxies which appear passive from a spectrum that samples only their bulge, but have also normal star-forming discs (Haines et al. 2008).

In figure 1 and figure 2, we plot the distribution of cluster galaxies in the CPPS depending on their star formation activity and luminosity. In figure 1, we show the whole galaxy sample split in two sub-samples of similar size for magnitudes brighter and fainter than  $M_{r'} = -19.5$  (this corresponds ap-

proximately to  $M_{r'}^* + 1.70$ , Blanton et al. 2003a). Figure 2 shows the complete cluster galaxy sample down to  $M_{r'} = -18.37$ . In order to enhance the statistics and taking advantage of the symmetry of clusters in the kinematic axis with respect to the average redshift, especially in the virial region, we merge the positive and negative quadrants of the CPPS in only one quadrant. We return to discuss the accuracy of this assumption later in this section, also see table 3. In addition, we mirror this quadrant with respect to both axes with the motivation that this approach makes the visualization, description and comparison of CPPS distributions between different galaxy populations, easier.

All density maps shown in this article are  $33$  bin  $\times$   $55$  bin two-dimensional histograms smoothed with a two-dimensional Gaussian kernel of  $\sigma(\tilde{r}) = \frac{5}{6}$  and  $\sigma(\tilde{s}) = 1$ . We choose this relatively large size of Gaussian kernel to derive more robust statistical properties and to dilute the galaxy substructures observed in galaxy clusters even near to the projected cluster center (Biviano et al. 2002). More important, our aim is studying the global CPPS distribution of clearly distinct galaxy populations e.g. passive vs. star-forming, more than to give a precise computation of the small-scale variations of the observed distributions of galaxy populations. Iso-density contours are equally spaced and divide the whole range of density for each CPPS distribution in six bins. With respect to the radius range shown in previous figures, we check that outside  $R_P = 0.9r_{200}$  the contribution of galaxies from neighboring clusters becomes noticeable.

In a first inspection to figures 1 and 2, the two galaxy populations show clearly distinct distributions. While the distribution of passive galaxies is clearly concentrated around the origin of coordinates  $(\tilde{r}, \tilde{s}) \sim (0, 0)$ , the distribution of star-forming galaxies is biased towards radii close to and outside the projected virial radius. On the contrary, the distribution of the two bins of different luminosity ranges,  $M_{r'} \leq -19.5$  and  $-19.5 < M_{r'} \leq -18.37$  of the same galaxy population (passive or star-forming) seem quite similar. In order to make a quantitative comparison of the CPPS distributions,  $\mathcal{D}(\tilde{r}, \tilde{s})$ , for the two luminosity bins of the same galaxy population, we apply a Kolmogorov-Smirnov (K-S) test to the CPPS distributions in the CPPS region delimited by  $0 < \tilde{r} < 0.9$  and  $0 < \tilde{s} < 3$ . The values for the probabilities and re-

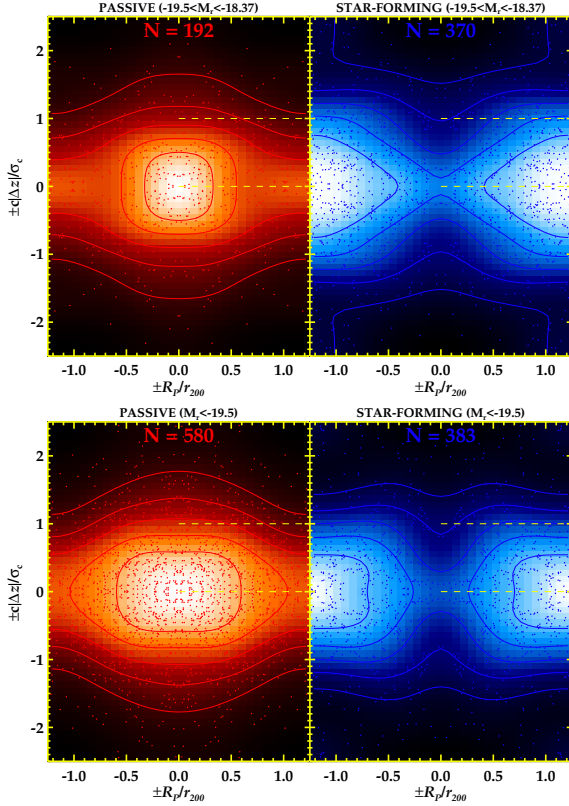


Fig. 1.— Stacked CPPS of low-luminosity ( $-19.5 < M_{r'} \leq -18.37$ ) (top panel) and high-luminosity ( $M_{r'} \leq -19.5$ ) (bottom panel) clusters galaxies. The diagrams are symmetrized with respect to both axes. Left (right) panel corresponds to passive (star-forming) galaxies. The intensity map corresponds to the CPPS density of galaxies and contours represent the lines of isodensity. Two parallel horizontal dashed lines are located at  $\tilde{s}=0$  and  $\tilde{s}=1$  only for comparison purposes. The numbers at the top indicate the numbers of galaxies which are in each quadrant of the plot.

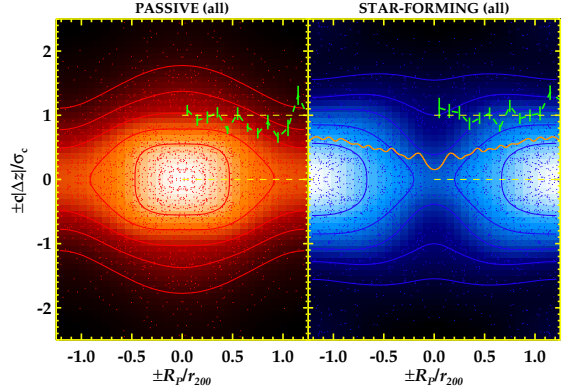


Fig. 2.— Stacked CPPS of the whole cluster galaxy sample. The broken dashed lines with uncertainty bars represent the radial profile of velocity dispersion and vertical bars are the bootstrap uncertainties in each bin. The solid line in the right panel shows the radial trend of the star-forming galaxy fraction (see the vertical axis as reference for numerical values). Color code, isodensity lines and the rest of elements of the figure are defined in the same way as figure 1.

spective uncertainties, that the two distributions come from the same parent function are quoted in table 2. The uncertainties here are computed assuming binomial uncertainties for the cumulative distribution functions of each data distribution. The purpose of including the uncertainties is showing the effect of the sample size in the accuracy of the K-S probabilities i.e. two distributions of very different sizes can give the same K-S probability but these two values should not be equally significant. Also, we show in table 3 the results of different K-S tests applied to CPPS distributions of galaxy populations in order to check the assumption of symmetry of clusters in the kinematic axis with respect to the average l-o-s velocity. These tests are described in the corresponding caption.

As can be shown in table 3 in all cases the K-S tests produce significant probabilities that each distribution and its 'reflected' counterpart come from the same parent function, except for the comparison (2) i.e.  $\mathcal{D}(\tilde{r}, \tilde{s} \geq 0) \sim \mathcal{D}(\tilde{r}, \tilde{s} < 0)$  of the star-forming population. This comparison produces a

Table 2: **Results from the Kolmogorov-Smirnov test to assess the similarity of the CPPS distributions of (passive and star-forming) galaxy populations in different luminosity bins:  $M_{r'} \leq -19.5$  (HL) and  $-19.5 < M_{r'} \leq -18.37$  (LL).**

GALAXY POPULATION	$\mathcal{D}_{HL}(\tilde{r}, \tilde{s}) \sim \mathcal{D}_{LL}(\tilde{r}, \tilde{s})$ (1)
PASSIVE	$69^{+18}_{-19}$ %
STAR-FORMING	$47^{+21}_{-17}$ %

**(1) K-S probability of  $(\tilde{r}, \tilde{s})$  2D distributions of high ( $M_{r'} \leq -19.5$ ) and the low-luminosity ( $-19.5 < M_{r'} \leq -18.37$ ) cluster galaxies come from the same parent 2D function.**

low but not negligible probability of  $4^{+5}_{-2}$  % which could be understood as an indication of some substructure in the population of passive galaxies.

Following the K-S probabilities shown in table 2, we can conclude that the CPPS distributions of the two luminosity bins are not statistically distinguishable for passive and star-forming galaxies. This result is in agreement with pre-

Table 3: **Results for the Kolmogorov-Smirnov test to assess the symmetry in the kinematic axis of the CPPS distributions.**

GALAXY POPULATION	(1)	$\mathcal{D}(\tilde{r}, +\tilde{s}) \sim \mathcal{D}(\tilde{r}, -\tilde{s})$
PASSIVE		$21^{+12}_{-8}$ %
STAR-FORMING		$19^{+12}_{-8}$ %
	(2)	$\mathcal{D}(\tilde{r}, \tilde{s} \geq 0) \sim \mathcal{D}(\tilde{r}, \tilde{s} < 0)$
PASSIVE		$4^{+5}_{-2}$ %
STAR-FORMING		$15^{+12}_{-7}$ %
	(3)	$\mathcal{D}(\tilde{r}, \tilde{s}) \sim \mathcal{D}(\tilde{r}, \pm \tilde{s} )$
PASSIVE		$84^{+10}_{-13}$ %
STAR-FORMING		$81^{+11}_{-14}$ %

**(1) Comparison between the  $\mathcal{D}(\tilde{r}, \tilde{s})$  and its ‘reflection’ with respect to the kinematic axis  $\mathcal{D}(\tilde{r}, -\tilde{s})$ . (2) Comparison between the positive  $\mathcal{D}(\tilde{r}, \tilde{s} \geq 0)$  and the negative side  $\mathcal{D}(\tilde{r}, \tilde{s} < 0)$  in the kinematic axis of  $\mathcal{D}(\tilde{r}, \tilde{s})$ . (3) Comparison between the  $\mathcal{D}(\tilde{r}, \tilde{s})$  and its collapsed and symmetrized counterpart  $\mathcal{D}(\tilde{r}, \pm|\tilde{s}|)$ .**

vious results in the literature that only found a distinct behaviour in the CPPS for the brightest galaxy/galaxies in clusters, as outline in the following. Biviano et al. (1992) found that galaxies brighter than the magnitude of the third-ranked object,  $m_3$ , have velocities lower than the average velocity of the remaining galaxies of the cluster. Biviano et al. (2002) find that luminosity segregation in the CPPS is evident only for the ellipticals that are outside galaxy substructures and which are brighter than  $M_R = -22$ . Goto (2005b) found that only the brightest  $M_z < -23$  cluster galaxies present a significantly smaller velocity dispersion than the  $M_z \geq -23$  galaxies, similar to what had been found in previous works (e.g. Adami et al. 1998b).

Given the results of table 2 which show no significant differences in the CPPS as a function of luminosity we plot in figure 2 all luminosities together. We then proceed to describe the CPPS distribution of passive galaxies. The isodensity contours of the CPPS distribution which encloses the bulk of the passive population presents a ‘peanut’ shape while in the innermost regions of the CPPS, the isodensity contour presents a ‘boxy’ shape. The CPPS distribution also shows a tail towards large radii which gets narrower in velocity space outside the virial region.

With regard to the CPPS distribution of the star-forming population, the isodensity contours have a convex triangular shape increasing in separation towards larger radii with a maximum in density around  $\tilde{s} \sim 0$  and  $\tilde{r} \gtrsim 1$  and they also shows a small but non negligible population of star-forming galaxies concentrated at the projected center of clusters  $\tilde{r} \sim 0$  and with low l-o-s velocities  $|\tilde{s}| \lesssim 0.5$ . This population of star-forming galaxies around  $(\tilde{r}, \tilde{s}) \sim (0, 0)$  could be linked with two possible origins: (1) it could be a population of star-forming galaxies which survive to the hostile environment of cluster virial regions. We discuss this possibility in subsections 4.2 and 4.3 or; (2) these could be galaxy interlopers mixed in projection in the virial region. In this respect, Diaferio et al. (2001) probe, in a set of simulated clusters, the fraction of galaxies that lie at physical distances larger than  $r_{200}$  as a function of projected clustercentric radius. At the centers of clusters, the interloper fraction with respect to the total sample is small, around 10%. The fraction of red

( $B-V > 0.85$ ) cluster members that are interlopers is even smaller,  $\sim 3\%$ . However, the fraction of blue cluster galaxies which are galaxy interlopers is higher than 50 per cent.

With respect to the fraction of star-forming galaxies, it presents a linear trend which goes from 20-30% at the cluster centers  $\tilde{r} \approx 0$  to a  $\sim 70\%$  for  $\tilde{r} \sim 1$ . This central value is in good agreement with a set of works which probes this quantity in virial regions of massive clusters (Poggianti et al. 2006; Popesso et al. 2007; Finn et al. 2008) whereas the fraction at the projected virial radius is even higher than the fraction of star-forming of  $\sim 50\%$  found in the field regions (e.g. Balogh et al. 2004; Rines et al. 2005). This higher fraction comes from the fact that we are showing a luminosity range which includes galaxies less luminous than these works. In fact, Haines et al. (2007) find that in the lowest density regions the fraction of star-forming galaxies increases steadily as luminosity decreases from a fraction of 50% for most luminous galaxies  $M_{r'} = -21.5$  to a fraction of virtually 100% for the less luminous bin around  $M_{r'} = -18$ .

Regarding the radial profiles of velocity dispersion, the star-forming galaxies show an approximately flat radial profile around  $\tilde{s} = 1$  up to a radius of  $\tilde{r} \sim 1$  while the passive galaxies present a mild negative slope in the radial profile which goes from  $(\tilde{r}, \tilde{s}) \approx (0, 1)$  to  $(\tilde{r}, \tilde{s}) \approx (1, 0.7)$ . We consider that the last point at  $\tilde{r} \sim 1.15$  is contaminated by nearby clusters as mentioned in the beginning of this subsection.

Given that the bootstrap uncertainties in this work are of the order of 10-15%, we say that the kinematic behaviour of passive and star-forming galaxies are not distinguishable inside most parts of the virial region, except for a small decrease in velocity dispersion of passive galaxies around  $R_P = r_{200}$ . The first statement alone would them suggest that both passive and star-forming galaxies are approximately virialized inside the virial region, as it was also pointed out by previous authors (see Biviano & Girardi 2003, and references therein), whereas the decrease of velocity dispersion for passive galaxies around  $R_P = r_{200}$  could be explained by the contribution of backplash galaxies. Simulations show that these galaxies present a more centrally peaked velocity histogram in contrast with that for the infalling galaxies, which present a velocity peak well apart from the cluster

average l-o-s velocity (e.g. Gill et al. 2005).

It is worth mentioning that Goto (2005a) found that the family broadly identified as star-forming late-type blue galaxies have a systematically larger velocity dispersion than that for the family composed by the passive late-type red galaxies. Specifically, the largest difference is found between the star-forming population  $\langle \tilde{s} \rangle = 1.128$  and the passive population  $\langle \tilde{s} \rangle = 0.960$ , when they are splitting them by their star formation rate (SFR) at  $\text{SFR}(\text{H}\alpha) = 2 \text{ M}_{\odot} \text{ yr}^{-1}$ . This difference decreases when the sample is split by color, where  $\langle \tilde{s} \rangle = 1.085$  for the blue  $u' - r' < 2.22$  population and  $\langle \tilde{s} \rangle = 0.961$  for the red  $u' - r' \geq 2.22$  population. This trend found by Goto (2005a) suggests that the kinematic behaviour of star-forming galaxies shows a larger difference with respect to the passive galaxies when they show a more intense star-formation activity as also we show in subsection 4.3.

### 3.2. Clusters from the Millenium Simulation in the CPPS

Taking into account the distribution of simulated galaxies in the CPPS depending on the time when they were accreted by their parent cluster, Haines et al. (2012) were able to identify two broad categories of galaxies, those galaxies accreted at an early epoch and those accreted after the formation of the core. The first category is well concentrated at the cluster center and with low l-o-s velocities suggesting a longer life settled at the cluster core. The second category is composed by one population of infalling galaxies and another population of galaxies which have completed their first pericenter and are now moving outward which are the so-called bound backplash galaxies (Mamon et al. 2004; Gill et al. 2005; Pimblet 2011). Therefore, taking advantage of the CPPS to distinguish the accretion epoch of a specific galaxy depending on its location in the CPPS and also, considering the clusters are hostile environments to the star-formation activity, we proceed to study the similarities and differences between (i) the CPPS distributions of passive and star-forming galaxy populations and (ii) the CPPS distributions of the accreted galaxy halo population and the non-accreted galaxy halo populations. We labeled the accreted galaxy halos as those galaxy halos which have passed inside a certain cluster-centric radius (e.g.  $r_{200}$ ) before an specific cosmic



epoch, for instance a look-back time of one Gyr, and the non-accreted halo population as those halos which are still outside this radius before this cosmic epoch. Within this approach, it is assumed that a star-forming galaxy after it is accreted inside the accretion radius eventually becomes a passively-evolving galaxy.

For this purpose, cosmic regions centred on 28 massive clusters ( $M_{200} > 2 \times 10^{14} h^{-1} M_{\odot}$ ) were extracted from the Millennium simulation (Springel et al. 2005). The 28 clusters were specially selected (1) to have clean caustics without significant contamination from background structures, and (2) to have velocity dispersions (for galaxies with  $R_P < r_{200}$ ) matching those of our observed cluster sample. In the simulated sample, there are three clusters which have velocity dispersions close to that of ABELL1185, while the remainder have velocity dispersions in the range 540-780  $\text{km s}^{-1}$  as it is shown in table 4 along with the masses and radii of the selected simulated clusters. We check that the observed and the simulated samples follow a similar trend in the  $r_{200}-\sigma_c$  and  $M_{200}-\sigma_c$  relations. The volumes extracted around each cluster were checked in the l-o-s direction in order to ensure that for a distant observer viewing along this axis, all galaxies with line-of-sight velocities within 3000  $\text{km s}^{-1}$  of the cluster redshift would be included, enabling us to fully account for projection effects.

The Millennium simulations (Springel et al. 2005) cover a  $(500 h^{-1} \text{Mpc})^3$  volume, and provide catalogs of dark matter halos and galaxies, the latter based on the semi-analytic models (GALFORM) of Bower et al. (2006), in which peculiar velocities, positions, absolute magnitudes and halo masses are given at 63 snapshots covering a look-back time range from  $t_{LB}=13.57$  Gyr to nowadays. The galaxy l-o-s velocities and sky positions for the 28 systems were stacked, setting the origin at the average l-o-s velocity  $cz_c$  and at the cluster center, respectively. Normalization by the velocity dispersion  $\sigma_c$  and the virial radius  $r_{200}$ , respectively, was then performed. Figure 3 shows the stacked CPPSs for simulated galaxies with  $M_K < -22.60$  (which corresponds to  $M_K^* + 2.36$ , Merluzzi et al. 2010) in the 28 simulated clusters, split into two categories depending on the accretion epoch and for two different values of accretion radius,  $r_{acc}=r_{200}$  (left) and  $r_{acc}=r_{500}$  (right).

Table 4: **Properties of the set of simulated clusters.**

ID	$\sigma_c(z=0)$ $\text{km s}^{-1}$	$r_{200}(z=0)$ Mpc	$M_{200}(z=0)$ $10^{14} M_{\odot}$
(1)	(2)	(3)	(4)
1	1034.21	2.452	17.187
2	1053.32	2.362	15.369
3	1046.45	2.084	10.560
4	708.94	1.762	6.377
5	755.39	1.814	6.955
6	732.22	1.964	8.831
7	706.66	1.737	6.111
8	769.25	1.925	8.317
9	726.60	1.965	8.844
10	738.52	1.884	7.803
11	656.06	1.766	6.417
12	692.45	1.815	6.976
13	780.00	1.542	4.276
14	634.93	1.494	3.891
15	602.94	1.510	4.011
16	661.52	1.383	3.088
17	689.75	1.487	3.833
18	732.29	1.529	4.166
19	621.70	1.530	4.174
20	659.68	1.468	3.691
21	653.14	1.463	3.654
22	603.12	1.557	4.401
23	559.93	1.559	4.419
24	707.28	1.528	4.163
25	537.35	1.516	4.066
26	714.62	1.456	3.598
27	731.48	1.469	3.698
28	712.86	1.430	3.413

**(1) ID number, (2) the velocity dispersions are computed including all galaxies which would be identified as cluster members via a spectroscopic survey within a projected radius  $R_P=r_{200}$ , (3) the halo radii  $r_{200}$  are calculated from the  $M_{200}$  and (4)  $M_{200}$  values are provided by the simulation.**

Assuming we do not find luminosity segregation in the CPPS for the whole cluster galaxy sample, it is fair to compare the observed sample with this sample of simulated galaxies showing a  $K$ -band luminosity range down to  $M_K^* + 2.36$ . This simulated sample is comparatively inside the observed  $r'$ -band luminosity range which reaches down to  $M_{r'}^* + 3.21$ . We show the three snapshots corresponding to the current cosmic epoch and the values of look-back time closer to 1 Gyr and 2 Gyr; these are  $\text{snap}=63$  (nowadays),  $\text{snap}=59$  ( $t_{LB}=1.13$  Gyr) and  $\text{snap}=56$  ( $t_{LB}=2.09$  Gyr). We choose this time step of  $\sim 1$  Gyr because it is a typical value for the crossing time for a galaxy in a massive cluster (Boselli & Gavazzi 2006). Furthermore, this time-scale is of the same order of magnitude than the time-scale of galaxy evolution of optical colors (Kennicutt 1998), such as  $u'-r'$  which is of interest in the study of the CPPS distribution of star-forming galaxies depending on their intensity of star formation, as shown in subsection 4.3.

In a first inspection of figure 3, one can notice that there is a qualitative agreement between the CPPS distribution of the observed galaxy populations in figure 2 and the simulated halo populations in figure 3. This suggests that the attempt to link the passive population with the accreted population and the star-forming population with the non-accreted population is a good approach.

With respect to the CPPS distribution of the accreted population (odd panels in figure 3), the isodensity contours present a round/elliptical shape in the virial region. In addition, the population inside the projected virial radius  $R_P < r_{200}$  is comparatively larger than the population outside the projected virial radius  $R_P > r_{200}$  as (a) one goes back in time i.e. longer look-back time of accretion and (b) larger accretion radius are considered i.e.  $r_{acc}=r_{200}$  instead of  $r_{acc}=r_{500}$ . In fact, for an accretion radius of  $r_{200}$  and when the accretion epoch is set to the current cosmic epoch, we have the largest population outside the projected virial radius  $R_P > r_{200}$  as compared to the population inside the projected virial radius  $R_P < r_{200}$ . Regarding the radial profile of velocity dispersion of accreted population, it shows a monotonic decrease towards large radii in all shown snapshots, which is in agreement with the results that find a more centrally peaked velocity distribution for

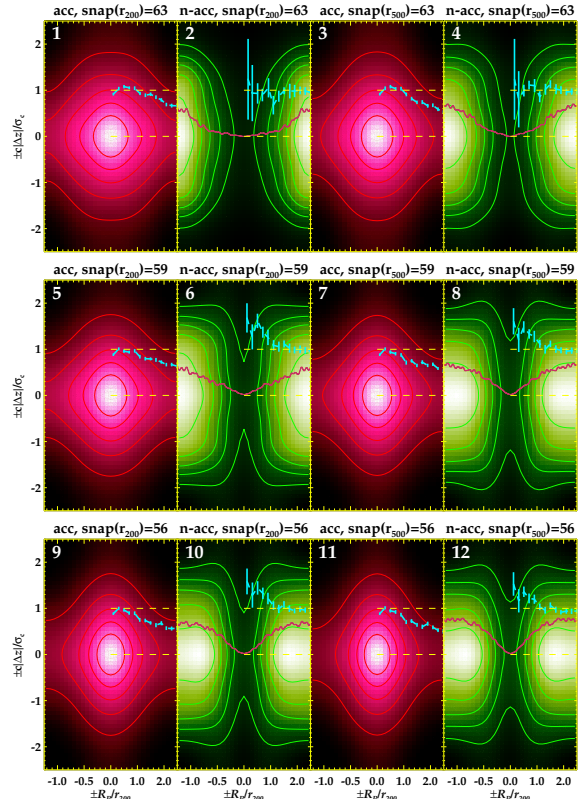


Fig. 3.— Stacked CPPS of a set of isolated galaxy clusters taken from the Millennium Simulation (Springel et al. 2005). The simulated population is split in two categories depending on if the simulated galaxy was accreted (odd panels for accreted one) or not (even panels for non-accreted one) and for two different radii where it is assumed the galaxy is accreted  $r_{acc}=r_{200}$  (two columns at the left) and  $r_{acc}=r_{500}$  (two columns at the right). See definition of accreted and non-accreted galaxy in the first paragraph of section 3.2. From top to bottom, the corresponding accretion epochs are the current cosmic epoch ( $\text{snap}(r_{acc})=63$ ), a look-back time of  $t_{LB}=1.13$  Gyr ( $\text{snap}(r_{acc})=59$ ) and  $t_{LB}=2.09$  Gyr ( $\text{snap}(r_{acc})=56$ ). In these graphs, the solid line shows the radial fraction of non-accreted galaxy halos. The rest of elements of the figure are defined in the same way as figure 2.

the backplash population (Gill et al. 2005). This profile also shows a small dip at  $\tilde{r}\sim 0$ .

Regarding the CPPS distribution of non-accreted population (even panels in figure 3), it presents a maximum around  $(\tilde{r}, \tilde{s})\sim(1,0)$  which is relatively round for a current cosmic epoch of accretion and an accretion radius of  $r_{acc}=r_{200}$  while it becomes more ‘boxy’ for longer look-back times of accretion and smaller accretion radii. The non-accreted population occupies more inner parts of virial region when it is considered a smaller accretion radius ( $r_{500}$ ) and longer look-back times of accretion. Regarding the radial profile of velocity dispersion (dashed line with uncertainty bars), it changes from a flatter profile when the accretion epoch is nowadays to a radial profile showing an increase around  $\tilde{r}\sim 0$  for earlier accretion epochs. The radial fraction of the non-accreted population (solid line in figure 3) goes from a very low value lower than 3% at the projected cluster center to around 60% at  $R_P\sim 1.25r_{200}$  in the case the accretion radius  $r_{acc}=r_{200}$  and it reaches around 70% in the case the accretion radius  $r_{acc}=r_{500}$ . We point out the presence of non-accreted haloes inside the virial radius  $R_P<r_{200}$  at all shown snapshots and in some cases, even in the low velocity interval  $\tilde{s}\sim 0$ .

#### 4. Discussion: Similarities and differences between the CPPS distributions of the galaxy populations and the halo populations

In the attempt to link the distribution of accreted halos with the passive galaxies and the distribution of non-accreted halos with the star-forming galaxies, we consider the distribution of accreted/non-accreted galaxy halos in the case of  $\text{snap}(r_{200})=63$  as the most similar distribution to the passive/star-forming galaxies. We are taking into account that this is the snapshot where (i) the contribution of the accreted population outside the projected virial radius  $R_P>r_{200}$  to the whole accreted population is the largest of the cases shown here and the most similar to the contribution of the passive population outside the projected virial radius  $R_P>r_{200}$  to the whole passive population and (ii) the radial profile of velocity dispersion and the range of l-o-s velocities of non-accreted halos inside the virial radius

$R_P<r_{200}$  are the most similar to those ones of star-forming galaxies. On the other hand, where we do not find a good match is in the fraction of non-accreted population near the projected center which is lower than 3% and is clearly lower than the corresponding fraction of star-forming galaxies of 20-30%. This difference could be explained if the star-forming galaxies inside the physical virial region  $r<r_{200}$  retain a remaining star formation activity. This possibility is discussed in subsections 4.2 and 4.3. Further, the non-accreted population covers a larger l-o-s velocity range than the star-forming galaxies. Gas stripping can be invoked to alleviate this difference. This will be discussed in subsection 4.2. Although there is clearly a qualitative similarity between the CPPS distributions of the accreted population and the passive population especially in the case of  $\text{snap}(r_{200})=63$ , they are quantitatively distinguishable. Specifically, a K-S test applied to both CPPS distributions i.e the simulated case of  $\text{snap}(r_{200})=63$  and the observed passive population produces a negligible probability that these ones come from the same parent function i.e.  $\mathcal{D}(\text{accreted})\sim\mathcal{D}(\text{passive})\lesssim 0.18\%$ .

At this point, we outline two caveats in the one-to-one identification of the accreted population with the passive population and the non-accreted population with the star-forming population. First, the non-accreted galaxy population is composed by both star-forming and passive galaxies in a mix determined by the typical galaxy population from the field. In the rarefied field, Haines et al. (2007) found the fraction of passively-evolving galaxies is a strong function of luminosity, decreasing from 50 per cent for  $M_{r'}\lesssim -21$  to zero by  $M_{r'}\sim -18$ . Secondly, the accreted galaxy population, as we see later in subsection 4.2, does not have to be necessarily solely identified with the passive galaxy population. In any case, it is observationally found that even the regions with the highest volume densities of galaxies show a fraction of  $\sim 30$  per cent of star-forming galaxies regardless of luminosity (Haines et al. 2007, see fig. 3).

On the comparison of the accreted population and the passive one, the most striking difference is the shape of the isodensity contours where they are elliptical or well rounded in the case of the accreted population and clearly ‘boxy’ or with a character-

istic ‘peanut’ shape for the observed distribution. Assuming the distribution in the CPPS is a combination between the radial profile of projected density and the velocity distribution of galaxies, we proceed to derive these two observables in order to know where the differences come from. For both data and simulations, the radial profiles of projected density are shown in figure 4 while the velocity histograms are shown in figure 5.

By comparing the radial profiles of projected density for the observed and simulated populations shown in figure 4, we find that both populations are well characterized by a broken power law  $\Sigma_P \propto \tilde{r}^\alpha$  within the uncertainties. The star-forming population seems to follow a simple power-law behaviour along the whole range of radii under consideration i.e. the virial region, while the passive population shows a break at  $R_P \sim 0.4r_{200}$ . In the case of the simulated clusters, the projected density profiles of the non-accreted population present approximately a simple power-law behaviour along the virial region and the accreted population shows a break at  $R_P \sim 0.5r_{200}$ . Specifically, the fits to radial profiles produce the following logarithmic slopes which are shown in table 5.

Table 5: **Logarithmic slopes of the radial profiles of projected density for the galaxy and halo populations studied here.**

Cluster sample		
	PASSIVE	STAR-FORMING
$\tilde{r} < 0.4$	$\alpha = -1.060 \pm 0.065$	$\alpha = -0.742 \pm 0.055$
$\tilde{r} > 0.4$	$\alpha = -1.57 \pm 0.12$	
Millennium simulation		
	ACCREDITED	NON-ACCREDITED
$\tilde{r} < 0.5$	$\alpha = -1.187 \pm 0.022$	$\alpha = 0.354 \pm 0.081$
$\tilde{r} > 0.5$	$\alpha = -2.695 \pm 0.094$	

As one can see in table 5, the radial profile of the passive population shows an inner slope very close to  $\alpha = -1$ , which implies a flat radial profile in number density (i.e. the number of galaxies per unit radius remains constant) and this seems to be the main cause of the ‘boxy’ and/or ‘peanut’ shape of isodensity contours of the passive population. Inspecting the top graph of figure 4, the inset lines for the comparison of slopes show that

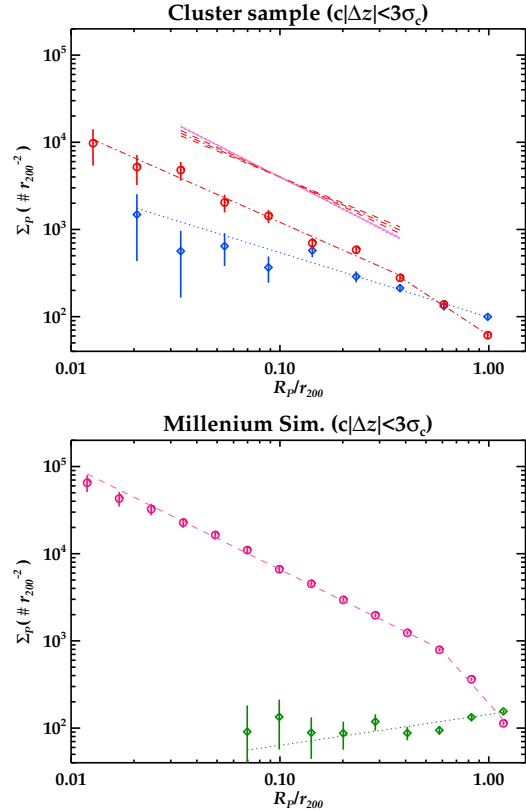


Fig. 4.— **Top graph:** Radial profile of the projected density (in natural units) of cluster galaxies. Circles correspond to passive galaxies while diamonds correspond to star-forming galaxies, including poissonian uncertainties as vertical bars. Dot-dashed and dotted lines through the data are power-law fits to the passive and the star-forming population, respectively. Solid and dashed lines above the data, including uncertainties in slopes shown as tilted lines around them, are respectively the fits to the simulated accreted and observed passive populations. **Bottom graph:** Radial profile of the projected density of accreted (circles) and non-accreted (diamonds) galaxy halos, including poissonian uncertainties. Dashed and dotted lines are power-law fits to the simulated accreted and non-accreted populations, respectively.

the radial profile slope of the accreted population is marginally steeper than that for passive galaxies

assuming the size of slope uncertainties. Further, the bias produced by uncertainty in cluster centering is able to reduce the logarithmic slope of radial profile of accreted halos enough to match the slope of the observed radial profile of passive galaxies in the innermost part of the virial region. We discuss this issue in depth in subsection 4.1.

As referred to the density profile of non-accreted haloes, the relatively low density of non-accreted haloes with respect to the star-forming population inside the virial radius suggests that we need a contribution of accreted haloes surviving inside the virial radius with a remaining of star formation as we discuss in subsections 4.2 and 4.3.

With regard to the distributions of l-o-s velocities, we fit a function in figure 5 of the form of an exponential with the negative branch of a vertical hyperbola as argument i.e.:

$$N_0 \exp \left\{ s_1 \left( 1 - \left( 1 + (\tilde{s}/s_0)^2 \right)^{1/2} \right) \right\}$$

obtaining for the passive population:

$$N_0=159\pm 11, s_1=2.4\pm 1.7 \text{ and } s_0=1.16\pm 0.54.$$

For the accreted population we obtain:

$$N_0=369\pm 11, s_1=3.00\pm 0.96 \text{ and } s_0=1.43\pm 0.29.$$

Taking into account the uncertainties in velocity histograms, it is not easy to establish a connection between the l-o-s velocity distributions of passive galaxies and the accreted halos but it is significant that both velocity distributions approximately follow an exponential law  $N \approx \exp(-\frac{s_1}{s_0} \tilde{s})$  for an intermediate velocity range  $0.5 \lesssim \tilde{s} \lesssim 2.5$ . Although, the parameters obtained from fitting to the velocity distributions of the passive and accreted populations are noticeably different, the shapes of fitted functions are compatible within uncertainties, as can be seen in figure 5. It is clear that these two parameters present some correlation between them.

On the relation of the shape of the velocity distribution with the type of galaxy orbits, Merritt (1987) derived the velocity distribution of galaxies in three extreme cases where the orbits are circular, radial or isotropic; finding a more cuspy distribution in the radial case, a bell-shaped distribution in the isotropic case and flat-topped distribution for the circular (see also van der Marel et al. 2000). Although, a number of studies found a very low or negligible anisotropy at the center of the clusters (e.g. Biviano & Katgert 2004;

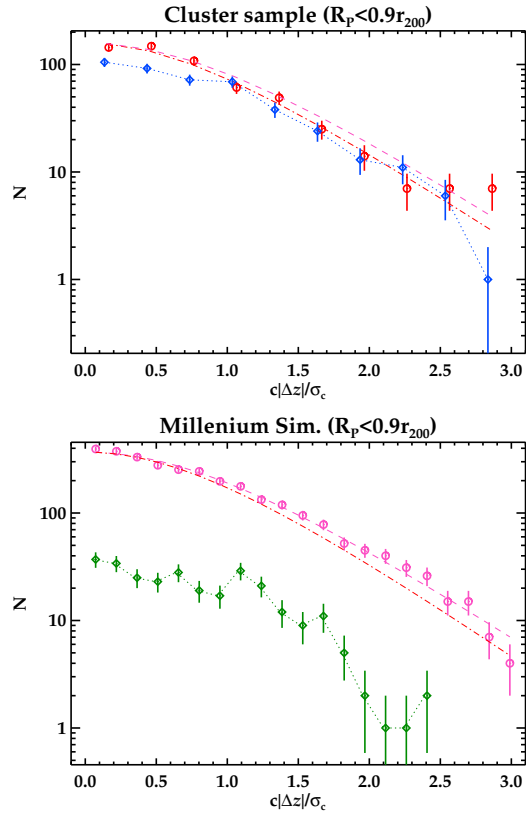


Fig. 5.— **Top panel:** Histograms of l-o-s velocity (in natural units) of passive (circles) and (diamonds) star-forming galaxies. **Bottom panels:** Histograms of l-o-s velocity (in natural units) of accreted (circles) and (diamonds) non-accreted galaxy halos. The dashed-dot and dashed lines are fits (see text for details) to the velocity distributions of passive and accreted population, respectively. In both panels, the fitted functions are scaled to the central value  $N_0$  to make easier the comparison between them. Dotted lines are just joining the data points of star-forming and non-accreted velocity distributions.

Hwang & Lee 2008; Wojtak & Lokas 2010), it is worth noting that the contribution of galaxy substructures is non negligible even at the very center (Biviano et al. 2002, fig. 3), which complicates the relation between the velocity distribution and the kinematic state of galaxy population. In addition, even in the case of large samples of clusters, the ve-

locity histograms of clusters show differences from Gaussian curves (Blackburne & Kochanek 2012).

From the comparison of the radial profiles of the projected density and the velocity distributions between the passive and the accreted populations, we can conclude that the differences in the isocontour shape between the passive population and the accreted one mainly come from the difference on the inner slope of the radial profile of projected density.

#### 4.1. Effects of uncertainties from cluster centering in the radial profile of projected density and the uncertainties of cluster average velocity in the velocity distribution.

The uncertainties in the determination of cluster center produce an unavoidable bias in the estimation of the central value of the profile of projected density toward lower values, such as it was pointed by Beers & Tonry (1986). On the comparison of the radial profiles of projected density between data and simulations, we have to take into account this bias. In order to estimate the importance of this bias depending on the uncertainty size, we take the set of simulated clusters as fiducial models and include the uncertainties of cluster centering and also, on the average l-o-s velocity of the cluster as it is described just below.

For each cluster labeled as  $j$ , we add uncertainties  $\delta\tilde{r}_j$  to the actual clustercentric radii  $\tilde{r}_i$  of galaxy labeled as  $i$  to obtain the ‘observed’ radius  $\tilde{r}_i^*$  using the following expression derived from simple trigonometric relations:

$$(\tilde{r}_i^*)^2 = (\tilde{r}_i)^2 + (\delta\tilde{r}_j)^2 - 2 \cdot \tilde{r}_i \cdot \delta\tilde{r}_j \cdot \cos(\theta_j - \theta_i)$$

with  $\delta\theta_{ji} \equiv \theta_j - \theta_i$  being the angle difference between  $\theta_j$ , the polar angle of vector  $\delta\tilde{r}_j$ , and  $\theta_i$ , the polar angle of vector  $\tilde{r}_i$ . Assuming that  $\theta_i$  is statistically independent of  $\tilde{r}_i$ , we can randomly generate  $\delta\theta_{ji}$  following an uniform distribution  $\mathcal{U}$  in all directions, i.e.  $\delta\theta_{ji} \sim \mathcal{U}_j [0, 2\pi]$  and the uncertainty  $\delta\tilde{r}_j$  can be generated following the modulus of a normal distribution i.e.  $\delta\tilde{r}_j \sim \|\mathcal{N}(0; \sigma_{\tilde{r}} [r_{200}])\|$ . In addition, we also test the effect of the uncertainty in the estimation of the average l-o-s velocity of the cluster  $\delta\tilde{s}_j$  over the actual cluster-frame l-o-s velocity  $\tilde{s}_i$  of galaxy  $i$  as:

$$\tilde{s}_i^* = \tilde{s}_i + \delta\tilde{s}_j$$

We model this effect assuming a normal distribution for the uncertainty  $\delta\tilde{s}_j$  to compute the ‘observed’ cluster-frame l-o-s velocity  $\tilde{s}_i^*$  i.e.  $\delta\tilde{s}_j \sim \mathcal{N}(0; \sigma_{\tilde{s}} [\sigma_c])$ . The result of 100 trials, using these inputs for both the radial profile of projected density and the velocity histogram, is summarized in figure 6.

As one can see in figure 6 for the case of the radial profile of the projected density, the fact of not exactly centering the profile produces a systematic underestimation of the central density. Regardless the importance of the bias, this is induced in a differential way along the radial range i.e. the bias is more intense in the innermost regions with a radius scale of the order of the average uncertainty. This produces a more pronounced curvature in the radial profile. Comparing the ‘observed’ radial profile of accreted halos including centering uncertainties with the radial profile of passive galaxies, we can derive that a relative uncertainty of around  $0.2r_{200}$  is enough to get the inner slope of radial profile of passive galaxies taking as parent distribution the radial profile of accreted halos. With respect to the l-o-s velocity histogram; it is required large values of uncertainty in the average l-o-s cluster velocity, well larger than a  $0.2\sigma_c$ , to produce a noticeable departure from the parent distribution. One of the simplest conclusions that we can derive from this computational test is that the induced bias is only significant in the case when the uncertainty is of the order of the typical scale of variation of the function under study, as it was pointed out by Adami et al. (1998c).

The uncertainties involved in the center and the average l-o-s velocity of clusters derived through the caustic method present an standard deviation of around  $100 \text{ km s}^{-1}$  in l-o-s velocity and around  $100h^{-1} \text{ kpc}$  in the projected center on the sky (Diaferio 2013, private communication) but the departure from actual center and average l-o-s velocity can reach values of  $0.5h^{-1} \text{ Mpc}$  on the sky and  $400 \text{ km s}^{-1}$  along the line of sight, respectively (Serra & Diaferio 2013). Moreover, the comparison of caustic centers with the X-ray emission peaks of the intracluster medium (ICM) produces differences of the order of  $150 \text{ kpc}$  (Rines & Diaferio 2006). In one hand, comparing these centering uncertainties with the values of virial radius in our cluster sample  $r_{200} \sim 1.2-2.3 \text{ Mpc}$  (see table 1), we can conclude that these val-

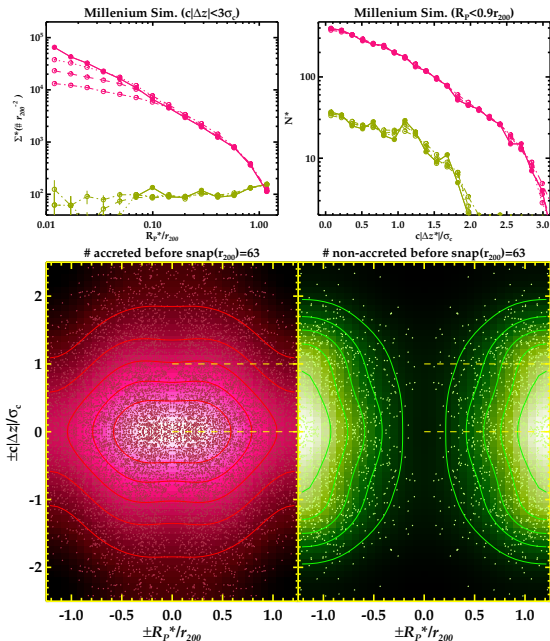


Fig. 6.— Illustration of the effect of adding uncertainties to the cluster centering (top left and bottom panels) and to the average l-o-s velocity (top right panel) in the case of  $\text{snap}(r_{200})=63$  (top left panel in figure 3). Top left panel: Radial profiles of projected density when it is added  $0.05r_{200}$  (dotted line),  $0.1r_{200}$  (dashed line) and  $0.2r_{200}$  (dot-dashed line) of uncertainty in cluster centering from top to bottom, respectively. Top right panel: Velocity distributions when it is added  $0.05\sigma_c$  (dotted line),  $0.1\sigma_c$  (dashed line) and  $0.2\sigma_c$  (dot-dashed line) of uncertainty in cluster average l-o-s velocity. In both top graphs, the filled circles joined with solid lines are the ‘unperturbed’ profiles. Bottom graphs: Stacked CPPS of the set of simulated galaxy clusters in the case of  $\text{snap}(r_{200})=63$  including a  $0.2r_{200}$  of uncertainty just in cluster centering. The rest of elements of the figure are defined in the same way as figure 3.

ues of uncertainty could explain the difference between the inner logarithmic slope of passive galaxies and the corresponding one of the accreted halos. This allows to assume that the bulk of passive

galaxies in the innermost parts of virial region are accreted galaxy halos. Adami et al. (1998c) simulate the effect of centering uncertainties using a NFW profile (Navarro et al. 1997) with an inner slope of  $\alpha \sim -0.66$  and do not find a significant decrease in the central projected density. Also, they find that the NFW profiles fitted to individual clusters, according to the likelihood ratio statistic, are generally not statistically distinguishable from the prototypical core profile, the King profile. Further, a King profile is favoured for the observed radial profile of the composite cluster sample at the innermost radii. As Adami et al. (1998c) argue the centering uncertainties tend to destroy the cusp in composite profiles. We add that this effect is stronger in cuspy profiles with a pronounced logarithmic slopes as indicate the results shown here. This differential behaviour between core profiles and cuspy profiles becomes more evident when the centering uncertainties are of the order of the core radius. In short, the differences in the effect of centering uncertainties between the test made by Adami et al. (1998c) and our test come from the fact that we test with a clearly more cuspy profile ( $\alpha \sim -1.19$ ) than their test which was performed with a core profile. At this point, we have to mention that there are noticeable differences in the inner slope between different semi-analytic models (Budzynski et al. 2012) and the effect of cluster centering uncertainty is greater for higher values of the inner slope. On the other hand, comparing the typical uncertainty of the average l-o-s cluster velocity  $cz_c$  with the range of cluster velocity dispersions  $\sigma_c \sim 500-1000 \text{ km s}^{-1}$ , this produces around a  $0.1-0.2r_{200}$  relative uncertainty, which is not enough to clearly change the cluster velocity distribution, as one can be seen in figure 6.

What seems more significant, the appearance of the CPPS distribution of simulated galaxy haloes in the case of  $\text{snap}(r_{200})=63$  (see bottom panel in fig. 6) is quite similar to the CPPS isodensity contours of the passive population, when it is added an uncertainty of  $0.2r_{200}$  just in cluster centering. Comparing figures 2 and 6, it is easy to see that the inner isocontours of the accreted population become similar to those ones of passive galaxies showing this characteristic ‘peanut’ shape and specifically, the isocontour of highest density presents a relatively ‘boxy’ shape. The main difference between isodensity contours of the ac-

creted population with centering uncertainty and the passive population is observed at  $R_P > 0.7r_{200}$ , where the accreted population has two ‘open’ isocontours while the passive population has three ‘open’ isocontours. This difference likely comes from the fact that there is an important contribution of passive galaxies in the non-accreted population as it is observed in the rarefied field (Haines et al. 2007). In addition, the simulated clusters were specially selected to be isolated clusters with a very low or negligible contamination from nearby clusters, whereas the set of real clusters shows contribution from neighboring clusters in their surroundings (see figure 1 in Paper I). This two facts will comparatively increase the CPPS density of passive galaxies around  $R_P \sim r_{200}$  and consequently this will modify the shapes of contours of lowest density for accreted halos changing them to ‘open’ contours.

#### 4.2. Gas stripping in the modulation of the CPPS distribution of galaxy populations

Motivated by the hint provided by the scarcity of star-forming galaxies near the projected center  $\tilde{r} \sim 0$  for relatively high l-o-s velocities  $\tilde{s} \gtrsim 0.5$ , we proceed to explore the influence of the ram-pressure stripping in shaping the distribution of galaxies in the CPPS. We compute the ‘intensity’ of this environmental effect throughout the CPPS as the ratio of the ram-pressure  $P_{\text{ram}}$  over the anchoring gas pressure of a galaxy  $\Pi_{\text{gal}}$  (Gunn & Gott 1972). We model the gas density profile with the classical  $\beta$ -profile (Cavaliere & Fusco-Femiano 1976):

$$\begin{aligned} \rho_{\text{ICM}}(r) &= \rho_0 \left[ 1 + \left( \frac{r}{R_c} \right)^2 \right]^{-\frac{3}{2}\beta} \sim \\ &\sim \rho_0 \left[ 1 + (c\tilde{r})^2 \right]^{-\frac{3}{2}\beta} = \rho_0 \tilde{K}(\tilde{r}; c, \beta) = \rho_0 \tilde{K}(\tilde{r}) \end{aligned}$$

with  $\rho_0$  being the central ICM density,  $R_c$  the core radius of the  $\beta$ -profile and  $c \equiv (r_{200}/R_c)(\pi/2)$ , where we are assuming that the three-dimensional radius  $r$  scales with scatter as  $r \sim \frac{\pi}{2}R_P$ , in order to account for projection effects.

$$\left. \begin{aligned} P_{\text{ram}} &= \rho_{\text{ICM}} \times v_{\text{gal}}^2 \sim \rho_0 \tilde{K}(\tilde{r}) \times \tilde{s}^2 (3\sigma_c^2) \\ \Pi_{\text{gal}} &\sim \Pi_{\text{MW}} \end{aligned} \right\} \implies$$

$$\implies \eta = \frac{P_{\text{ram}}(\tilde{r}, \tilde{s})}{\Pi_{\text{MW}}} ; \quad \tilde{s}^2 \tilde{K}(\tilde{r}) = \eta \left( \frac{\Pi_{\text{MW}}}{3\rho_0\sigma_c^2} \right) \quad (1)$$

We take  $v_{\text{gal}}^2 \sim \tilde{s}^2 (3\sigma_c^2)$  as a proxy of galaxy velocity in the cluster frame and  $\Pi_{\text{MW}}$  as the anchoring gas pressure in the Milky Way as a representative value for galaxies. Finally, as a fiducial example, we take the derived values for cluster CL+0024 (Treu et al. 2003):  $R_c = 60$  kpc,  $r_{200} = 1.7$  Mpc,  $\beta = 0.475$ ,  $\rho_0 = 3 \cdot 10^{14} \text{ M}_{\odot} \text{ Mpc}^{-3}$ ,  $\sigma_c = 911 \text{ km s}^{-1}$  and  $\Pi_{\text{MW}} = 2.1 \cdot 10^{-12} \text{ N m}^{-2}$  as a reference for the restoring gravitational force per unit area (units of pressure) for a galaxy like the Milky Way (see also Abadi et al. 1999, fig. 2 and Boselli & Gavazzi 2006, fig. 18). For comparison, Treu et al. (2003) propose a ‘stripping radius’ of 0.5-1 Mpc for this galaxy cluster CL+0024, but this approach is not taking into account the kinematic axis. Further, Boselli & Gavazzi (2006) explore the dependence of the HI deficiency parameter of Virgo A galaxies on the synthetic observable  $(1/\theta) \times v_{l.o.s}^2$ , which provides a broad one-dimensional trend of ram-pressure intensity, with  $\theta$  the projected cluster radius in angular units and  $v_{l.o.s}$  the cluster-frame l-o-s velocity.

We make note of a number of caveats. First, we have to keep in mind that we are probing the effects of an environmental phenomenon which depends on at least six environmental variables (three spatial and three velocity components) in a projected two-dimensional diagram. Also, despite the fact that we apply a scaling factor of  $v_{\text{gal}} \sim \sqrt{3}\sigma_c$  to account for the galaxy velocity, a certain amount of scatter seems unavoidable. In the same way, the ICM density is assumed to be dependant on the three-dimensional radius  $r$  whereas we only have the projected component  $R_P$ , so we apply an average scaling of  $r \sim \frac{\pi}{2}R_P$ . Furthermore, we are stacking in the CPPS galaxy distributions, clusters with a range of velocity dispersions  $\sigma_c \sim 500\text{-}1000 \text{ km s}^{-1}$ , and a collection of galaxies with different anchoring pressures (Boselli & Gavazzi 2006, their fig. 18). Because of these handicaps, our motivation is to analyse the influence of ram-pressure stripping in modulating the CPPS galaxy distribution in a qualitative way, more than to compute a precise shape of the  $\eta$  function. Nevertheless, the comparison produces conspicuous results, as one can see in



figure 7, where we overplotted iso-contours with a representative set of values of stripping intensity in both the CPPS of real clusters and simulated clusters. This set of values attempts to account for (i) the range of variation of  $\eta$  due to the variation of physical variables involved in the stripping intensity formula:  $\Pi_{gal}$ ,  $\rho_0$ ,  $\sigma_c$  and (ii) the shape of the two-dimensional stripping intensity function  $\eta(\tilde{r}, \tilde{s})$  in the CPPS.

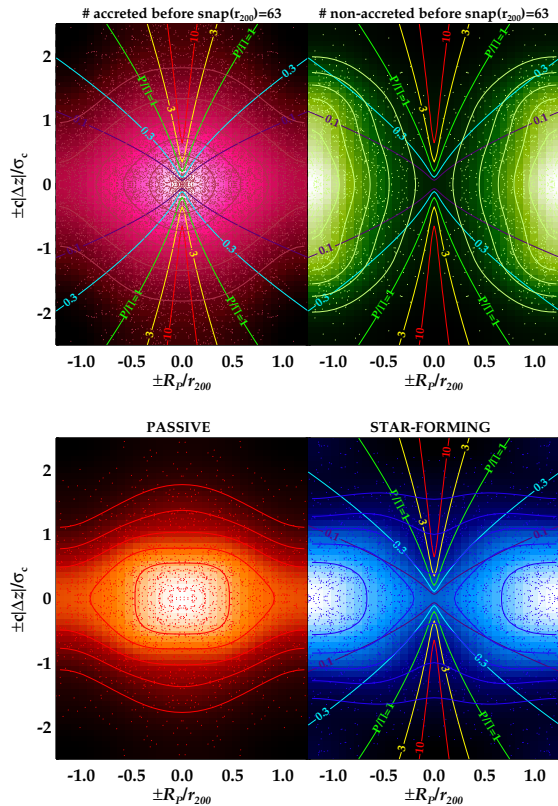


Fig. 7.— **Stripping intensity.** Isocontours of stripping intensity  $\eta = P_{ram}/\Pi_{gal}$  overplotted in the CPPSs of the halo populations in the case of  $\text{snap}(r_{200})=63$  (top) and the galaxy populations (bottom). Each contour is labeled by the ratio of ram pressure over the anchoring pressure of gas in the Milky Way  $\eta$  (see equation 1 and corresponding text for details) with this set of values  $\eta = [0.1, 0.3, 1, 3, 10]$ . The rest of elements of the figure are defined in the same way as figure 1.

In the case of simulated clusters (top panel of

figure 7) the region of lowest intensity (enclosed by purple iso-contours) is a region of the CPPS where the non-accreted galaxies are sheltered from ram-pressure gas stripping. In addition, the large range of l-o-s velocities exhibited by the non-accreted haloes in comparison with star-forming galaxies, could be modulated/reduced by the ram-pressure effect as one can see from the shapes of the contours of low stripping intensity  $\eta=0.1$  and 0.3. In this respect, a population of stripped non-accreted galaxy halos could be responsible for a decrease in the fraction of non-accreted star-forming galaxy population with respect to the whole non-accreted population. Furthermore, the fact that the galaxy population in the field contains an important contribution of passive galaxies (Haines et al. 2007) also reduces the fraction of the non-accreted star-forming galaxy population with respect to the whole non-accreted population. As the star-forming fraction and the non-accreted fraction present similar values around 60-70% in the surroundings of virial regions, the two facts outlined above implies that it would need a population of accreted galaxies with a remaining star formation currently located outside the virial radius.

Regarding the accreted halos, those star-forming galaxies which are infalling for the first time through these CPPS regions of low stripping intensity could survive as star-forming galaxies for a fraction of the cluster crossing time (i.e.  $\sim 1$  Gyr) before their gas reservoir would be exhausted, see subsection 4.3 in this respect. Further, those accreted galaxies which have never penetrated very deep in the virial region with high velocities could survive for longer periods of time as star-forming galaxies i.e. galaxies in circular orbits outside the innermost parts of the virial region. In this respect, while early spiral galaxies are in approximate isotropic orbits and the late spiral and emission-line galaxies are clearly biased toward radial orbits outside  $R_P \sim 0.7 r_{200}$ , there is a population of galaxies in substructures which seems to be in circular orbits at relatively large radii (Biviano & Katgert 2004).

As referred to the real clusters, the map of the stripping intensity presents a region of very high intensity for those galaxies close to the projected cluster center  $\tilde{r} \sim 0$  and with relatively high velocities  $\tilde{s} \gtrsim 0.5$  (red iso-contours in fig. 7), this

maximum of stripping intensity can explain the paucity of star-forming galaxies in this specific region of the CPPS. On the other hand, the region of very low stripping intensity (purple iso-contours in fig. 7) presents a triangular shape, increasing in separation towards larger radii and connected through a ‘bridge’ around  $(\tilde{r}, \tilde{s}) \approx (0, 0)$ . This allows to explain the presence of star-forming galaxies near to the projected cluster center, but only for those galaxies with relatively low l-o-s velocities. In this respect, assuming that the radial profile of projected-density along the transverse direction is similar to that along the l-o-s direction, the geometrical effects introduce a minor scatter (of the order of  $H_0 r_{200}$ ) in the l-o-s velocities i.e.  $(H_0 r_{200} / \sigma_c) \sim 12\%$ . Thus, the observed l-o-s velocity of galaxies near the projected center is a good proxy for the actual l-o-s velocity without much information about its position with respect to the cluster center. In consequence, those star-forming galaxies with relatively low l-o-s velocities at the projected center of clusters could come from any point along the transverse clustercentric distance. However, assuming that they retain a non negligible amount of star formation, it is quite likely that they are well outside of the innermost part of the virial region.

As can be derived from the comparison of iso-contours in the case of real clusters (bottom panel of figure 7), the stripping intensity  $\eta(\tilde{r}, \tilde{s})$  and the CPPS density of star-forming population are following opposite trends in the CPPS where (i) the maximum of  $\eta$  for  $\tilde{r} \sim 0$  and  $\tilde{s} > 0.5$  coincides with a scarcity of star-forming galaxies, (ii) the minimum for  $\tilde{r} > 1$  and  $\tilde{s} \lesssim 0.5$  coincides with the major concentration of star forming galaxies and (iii) there is a domain around  $(\tilde{r}, \tilde{s}) \sim (0, 0)$  showing a low stripping intensity and a significant density of star-forming galaxies. In particular, in the low l-o-s velocity interval  $\tilde{s} < 0.5$  of virial region, the stripping intensity strongly modulates the CPPS distribution of star-forming galaxies. This points out the map of stripping intensity as a modulation function which is acting over the distribution function in the CPPS.

As we have pointed out in the introduction, the effects of environmental processes are cumulative. Some of them can operate simultaneously quenching star formation in galaxies and these environmental processes operate with different time-

scales, regions of influence and varying their intensity depending on galaxy properties e.g. galaxy gravitational mass. This is one of the hypothesis with which we work in Hernández-Fernández et al. (2012b). Furthermore, only the appropriate observable can trace the effect of a specific environmental process. In this work, we probe the CPPS distribution of star-forming population and this space includes the proxies of the two physical variables which mainly determine the intensity of ram-pressure stripping i.e. cluster-centric radius and galaxy velocity. Therefore, the opposite trend in the CPPS between the density of star-forming population and the intensity of stripping clearly points out that the effect of ram-pressure stripping is a major contributor to quench the star formation in cluster galaxies in virial regions and in their close surrounding regions.

#### 4.3. Comparison between the CPPS distributions of intense and quiescent star-forming galaxies.

In this subsection, we probe the distribution of star-forming galaxies in the CPPS depending on the intensity of their star formation. A number of tests have been performed on the criterion to segregate between intense and quiescent star-forming galaxies in the two color-magnitude diagrams (NUV- $r'$  vs.  $M_{r'}$ ) and ( $u'-r'$  vs.  $M_{r'}$ ). These tests include a segregation based on fixed-color cuts and also tilted/curved lines in color-magnitude diagrams to account for the trend of ‘blue cloud’ towards bluer colors with decreasing luminosity (Wyder et al. 2007). The criterion applied  $u'-r'=1.8$  seems to be the one producing a clearer segregation between intense and quiescent star-forming galaxies in the CPPS. The result of the different criterion are shown in figure 8. From top to bottom and left to right, the criterion to segregate intense from quiescent star-forming galaxies are: (a)  $u'-r'=1.8$  attempts to split the star-forming population in two samples of similar size, (b)  $u'-r'=1.75-0.20(M_{r'}+20)$  traces the peak of the blue sequence along the observed range of  $r'$ -band luminosity, (c)  $NUV-r'=3$  separates the green valley from blue sequence with a unique color value, (d)  $NUV-r'=3.590+0.075(M_{r'}+20)-0.808 \tanh((M_{r'}+20.32)/1.81)$  separates the green valley from the blue sequence taking as reference the fit to the blue sequence

provided by Wyder et al. (2007).

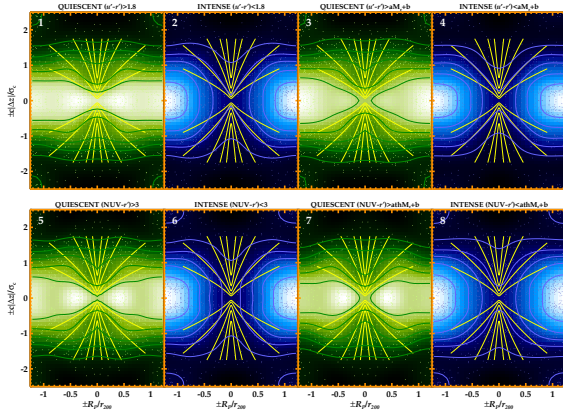


Fig. 8.— **Stacked CPPS diagrams for the star-forming population separated between the intense star-forming galaxies and the quiescent star-forming galaxies. From top to bottom and left to right, odd (even) panels represent quiescent (intense) star-forming galaxies split them by (a), (b), (c) and (d) conditions as it is described in subsection 4.3. Isodensity lines and the rest of elements of the figure are defined in the same way as figure 1 and contours of iso- $\eta$  have the same values that figure 7.**

The distribution of star-forming galaxies in the CPPS depending on their star-formation intensity shows two evident trends: (1) the intense star-forming galaxies are preserved outside the projected virial radius in the outer parts of the region of lowest stripping intensity and (2) the quiescent star-forming galaxies are distributed along the whole observed radial range and partially concentrated around two maxima, one maximum is located inside the projected virial radius but apart from the cluster center and the other maximum appears outside the projected virial radius. The first point suggests that the intense star-forming galaxies are those field galaxies with higher levels of star formation which have not yet suffered the star-formation quenching by the environment of cluster virial regions while the quiescent star-forming galaxies are shared between those field galaxies with lower levels of star formation and those star-forming galaxies showing a decline in their star formation due to the environmental effects of cluster virial regions. Accepting this de-

scription, in the case that the bulk star-forming galaxies were galaxy interlopers, an important fraction of intense star-forming galaxies would be observed inside the projected virial radius. In addition, the density of quiescent star-forming galaxies around  $(\tilde{r}, \tilde{s}) \sim (0, 0)$  shows a clear impact of the stripping phenomenon as is suggested by the similar trends of both the isodensity contours of quiescent galaxies and the iso-intensity contours of gas stripping in this region of the CPPS. These results reinforce the hypothesis that ram-pressure stripping is strongly influencing in the modulation of star formation history of cluster galaxies and specifically, of the star forming galaxies. We stress that this clear segregation in the CPPS between intense and quiescent star-forming galaxies is found applying different criteria about two colors,  $\text{NUV}-r'$  and  $u'-r'$ . In contrast, a so clear segregation is not found when the same sample of star-forming galaxies is split by their  $r'$ -band luminosity between high-luminosity ( $M_{r'} < -19.5$ ) and low-luminosity galaxies ( $M_{r'} > -19.5$ ), a galaxy property which strongly correlates with galaxy mass. Then, it is not expected that this segregation in the CPPS between intense and quiescent star-forming galaxies would come from differences in their stellar mass distributions. In this respect, Biviano et al. (2002) find that the different morphological types (E, S0, early and late spiral and emission-line galaxies) present different CPPS distributions but it is only found an evident luminosity segregation for the brightest  $M_R < -22$  ellipticals that are not in galaxy substructures.

In the top left panel of figure 8, it can be seen that the intense star-forming galaxies  $u'-r' < 1.8$  are mainly populating the space just outside the projected virial radius while the quiescent star-forming population  $u'-r' > 1.8$  is formed by those galaxies outside the projected virial radius and more remarkable, a population of galaxies clearly biased towards the center. We try to explain the most clear segregation between quiescent and intense star-forming galaxies splitting them at  $u'-r'=1.8$ , invoking a ‘synchronisation’ between two natural time-scales: the timescale of variation of visible color(s) (Kennicutt 1998) and the crossing time for clusters (Boselli & Gavazzi 2006) which are around  $10^9$  yr. This coincidence has the consequence that an infalling star-forming galaxy shows, by means of its visible color  $u'-r'$ , that

its star-formation activity is drastically diminished just when it would be well inside the cluster. This is only applied to those star-forming galaxies modestly attenuated, given that those star-forming galaxies highly attenuated appear in the red sequence (Wolf et al. 2009).

## 5. Summary and conclusions

We summarize the main results and conclusions of this work in the following paragraphs:

- There is no statistically significant luminosity segregation in the CPPS distribution of star-forming and passive galaxy populations along the observed luminosity range  $-23 \lesssim M_{r'} \lesssim -18$ .
- The passive population is concentrated around a unique maximum in the CPPS clearly centered at  $(\tilde{r}, \tilde{s}) \sim (0, 0)$  as it was found by previous works in the literature. The ‘boxy’ and/or ‘peanut’ shape of isodensity contours of passive population seems to be a direct consequence of a projected density radial profile varying with  $\sim \tilde{r}^{-1}$  in the innermost parts of the virial region. This radial trend can be mainly obtained from a more cuspy profile where the uncertainties in cluster centering are included.
- The star-forming population presents a maximum around  $(\tilde{r} \sim 0, \tilde{s} \gtrsim 1)$  showing an evident preference for environments outside the virial region and with lower l-o-s velocities. The significant fraction of star-forming galaxies at the projected center of clusters are mainly those galaxies with low l-o-s velocities and they can be mainly identified as those galaxies with a remaining star formation activity inside the physical virial region or, in a lower degree, as galaxy interlopers i.e. outside the physical virial region. The CPPS density of star-forming galaxies and the intensity of ram-pressure stripping  $\eta(\tilde{r}, \tilde{s})$  present an opposite trend throughout the CPPS. This opposite behaviour suggests there is a major contribution of ram-pressure stripping to the modulation of star-formation activity of galaxies in cluster virial regions and their close vicinity.
- The intense star-forming population is mainly located around a unique maximum outside the virial region and around  $(\tilde{r}, \tilde{s}) \sim (0, 1.25)$ . This region of the CPPS coincides with the outer part of the regions with lowest stripping intensity. The quiescent star-forming population is distributed in a more extended range of radii, also occupying the CPPS region of the lowest stripping intensity but as much inside the projected virial radius as outside the projected virial radius.
- In the cross-identification of the passive population with the accreted population and also, of the star-forming population with the non-accreted population, we find that:
  - the non-accreted population seems to make a major contribution to the star-forming population outside the virial region where the larger range in l-o-s velocity shown by the non-accreted population in comparison with the star-forming population can be reconciled taking into account the effect of the ram-pressure stripping. It would be needed a population of accreted galaxies with a remaining star formation inside the virial radius  $R_P < r_{200}$  to reach the fraction of star-forming galaxies inside the virial radius. Considering the similar fraction of the non-accreted population and the star-forming population outside the virial radius, it also would be needed a population of accreted galaxies with a remaining star formation outside the virial radius  $R_P > r_{200}$  in order to counteract a population of stripped non-accreted galaxies and the population of passive galaxies from the field i.e. non-accreted passive galaxies.
  - the inner logarithmic slope of the radial profile of projected density of accreted population  $\alpha \sim -1.19$  can be substantially reduced when are considered the uncertainties of cluster centering. This decrease in the inner slope can be enough to reach the value of the inner slope of the density profile of the passive population  $\alpha \sim -1$ . The veloc-

ity distribution of accreted and passive populations are similar within uncertainties. We can conclude that the accreted population can account for the bulk of the passive population at the innermost part of virial region.

- the star-forming population of the inner parts of virial regions appears to mainly come from that accreted population with a relatively low l-o-s velocity and a remaining star formation activity and also, come from the non-accreted population  $r > r_{200}$  which appears projected inside the projected virial radius  $R_P < r_{200}$  i.e. they are galaxy interlopers.

## Acknowledgements

J.D.H.F. acknowledges support through the FAPESP grant project 2012/13381-0. C.P.H. was funded by CONICYT Anillo project ACT-1122. A.D. acknowledges partial support from the INFN grant Indark and from the grant Progetti di Ateneo/CSP TO\_Call.2\_2012\_0011 ‘Marco Polo’ of the University of Torino. J.I.P. acknowledges support through Proyecto de Excelencia FQM7058 ‘Historia de formación estelar y evolución química de galaxias en entornos de diferente densidad’. C.M.d.O. acknowledges support through FAPESP project 2006/56213-9 and CNPq grant 305205/2010-2. J.M.V. acknowledges support from the project AYA2010-21887-C04-01 ‘Starbursts and their imprint in the cosmic evolution of galaxies’.

The formal acknowledgements to the resources used in this work can be read at: [www.sdss.org/dr6/coverage/credits.html](http://www.sdss.org/dr6/coverage/credits.html) for the Sloan Survey, [ned.ipac.caltech.edu](http://ned.ipac.caltech.edu) for the NED webpage and [galex.stsci.edu/GR6/?page=acknowledgments](http://galex.stsci.edu/GR6/?page=acknowledgments) for the GALEX mission.

## Appendix

It is widely known the handicap of the fiber collision in the Main Galaxy Sample of SDSS; two spectroscopic fibers cannot be placed closer than 55 arcsec on a given plate (Strauss et al. 2002). This produces a lack of completeness throughout the survey which could be dramatic in the case of highly crowded fields e.g. the central regions

of galaxy clusters. Park & Hwang (2009) computed the radial dependence (in angular units) of the completeness of the Main Galaxy Sample for a sample of Abell clusters. They found a radial trend which goes from the asymptotic value around 90 % well out of cluster regions up to a completeness in the interval of 75-80 % in the very center of clusters. Applying this completeness correction in galaxy clusters along the radial axis has the disadvantage of including, in both the numerator and the denominator of the completeness fraction, a galaxy population which is not a genuine cluster population. This can bias the estimation of the completeness for a genuine cluster galaxy sample.

In order to estimate this fraction in an unbiased way and test the trend of this fraction along the radial axis, we simulate a composite population of a massive cluster at redshift  $z=0.033$  embedded into a galaxy background population. We make the test at this redshift because most clusters in this work are around this redshift. We assume that the galaxy projected density of a cluster follows a generalized King profile with the physical parameters found by Abdullah et al. (2011):  $\gamma = -(2/3)$  and a median value for the core radius of  $R_c = 0.295 h^{-1}$  Mpc. So, the angular distance of 55 arcsec in unit of this core radius for a cluster at  $z=0.033$  is  $d(55) = 0.085 R_c$ . We apply an algorithm of rejection which mimics the algorithm proposed by Blanton et al. (2003b), rejecting with higher priority those objects with a larger set of neighbour distances smaller than the critical distance  $d=55$ . We tune the projected density of background objects to reproduce at large radii the average projected density of objects of the Main Galaxy Sample  $\Sigma \sim 190$  gal deg $^{-2}$  which correspond to a projected density of  $\Sigma \sim 6.5$  gal  $R_c^{-2}$  in natural units. The richness of the cluster is fixed to  $\sim 250$  galaxies inside the  $r_{200}$  taking as reference ABELL 1185 from the set of clusters under study in this work. The stacked result from 50 trials is summarized in figure 9.

In a first inspection, the completeness of the composite (cluster+background) population follows a similar trend to the one found by Park & Hwang (2009) which has a mean value of 75-80 % at the very center of the cluster, whereas it shows an asymptote around 90 % at large radii. In this simulated trial, the trend of clustercentric

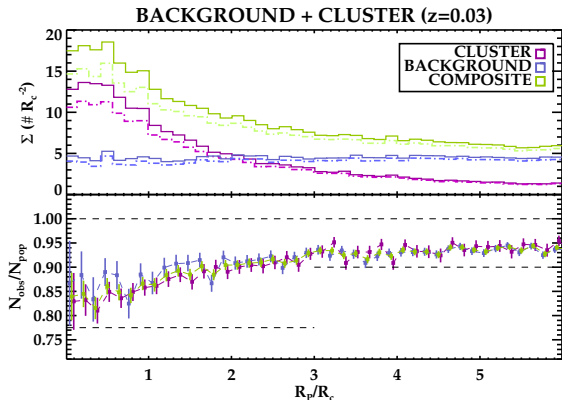


Fig. 9.— Simulated completeness of the Main Galaxy Sample depending on cluster-centric radius in core radius unit  $R_c$ . Top graph: Radial profiles of projected density from each population; cluster (purple), background (blue) and composite (green). The dark solid histograms correspond to the whole population and the light dashed histograms are the non-rejected population. Bottom graph: Completeness of each population with respect to its own total population. The lines including binomial uncertainty bars are the fractions of the non-rejected population over its own total population. Dashed flat lines mark the 90 and 77.5% which are the tendencies for small and large radii found in Hwang & Lee (2008). Also, it is shown a dashed line at 100% for comparison purposes.

completeness shows a bias of around 5 per cent toward higher values with respect to the one found by Park & Hwang (2009). Given that we deal with a background population of uniform density without any contribution of galaxy substructures, we attribute the lower completeness in the real sample to the presence of galaxy pairs and groups. This is not just easily applied to the field well outside the clusters, where there is a significant contribution of galaxy pairs and groups to the whole galaxy population (Cox 2000), but also at the very cluster center, where it is found a small contribution of galaxy substructures to the cluster population (Biviano et al. 2002).

The completeness in the three populations shows a monotonic decreasing trend with pro-

jected density as it would be expected. Specifically in the case of the composite population, the completeness decreases from 93-94% for a density of  $\Sigma \sim 6.5 \text{ gal } R_c^{-2}$  to a completeness of around 85%, this is a reduction of around a 10%, for a density approximately three times higher,  $\Sigma \sim 18 \text{ gal } R_c^{-2}$ . Along the radius range under  $R_c=2$ , the cluster completeness is not only systematically lower than the completeness from the composite population but also the completeness of the background population. It would be explained assuming a composite population where two populations with two different projected densities are mixed together: (1) as the projected density increases, the number of objects with neighbour distances smaller than the critical distance increases, (2) in a composite population, a new and different set of links smaller than the critical distance between objects from the two populations is established, (3) in these newly established links, the algorithm will penalize with higher priority the objects from a population with a higher density than the objects from a population with a lower projected density.

From this simple test, we can conclude that a genuine cluster population on top of a background population does not show a very different completeness from the composite population, assuming the range of galaxy projected densities similar to those we are working with. Indeed, for higher redshifts the apparent size of a cluster will be reduced and in consequence, the galaxy projected densities should be large for a cluster galaxy sample with an equivalent completeness limit in luminosity. In addition, the projected density of the background population also increases for the fainter completeness limits which are required for observations at higher redshifts. These two facts contribute to reduce the completeness of the non-rejected populations.

## REFERENCES

- Abadi, M. G., Moore, B., & Bower, R. G. 1999, MNRAS, 308, 947
- Abdullah, M. H., Ali, G. B., Ismail, H. A., & Rassem, M. A. 2011, MNRAS, 416, 2027
- Adami, C., Biviano, A., & Mazure, A. 1998a, A&A, 331, 439

- Adami, C., Mazure, A., Biviano, A., Katgert, P., & Rhee, G. 1998b, *A&A*, 331, 493
- Adami, C., Mazure, A., Katgert, P., & Biviano, A. 1998c, *A&A*, 336, 63
- Adelman-McCarthy, J. K., Agüeros, M. A., Allam, S. S., et al. 2008, *ApJS*, 175, 297
- Bahé, Y. M., McCarthy, I. G., Balogh, M. L., & Font, A. S. 2013, *MNRAS*, 430, 3017
- Balogh, M., Eke, V., Miller, C., et al. 2004, *MNRAS*, 348, 1355
- Beers, T. C. & Tonry, J. L. 1986, *ApJ*, 300, 557
- Bianchi, L., Rodriguez-Merino, L., Viton, M., et al. 2007, *ApJS*, 173, 659
- Biviano, A. & Girardi, M. 2003, *ApJ*, 585, 205
- Biviano, A., Girardi, M., Giuricin, G., Mardirossian, F., & Mezzetti, M. 1992, *ApJ*, 396, 35
- Biviano, A. & Katgert, P. 2004, *A&A*, 424, 779
- Biviano, A., Katgert, P., Mazure, A., et al. 1997, *A&A*, 321, 84
- Biviano, A., Katgert, P., Thomas, T., & Adami, C. 2002, *A&A*, 387, 8
- Blackburne, J. A. & Kochanek, C. S. 2012, *ApJ*, 744, 76
- Blanton, M. R., Hogg, D. W., Bahcall, N. A., et al. 2003a, *ApJ*, 592, 819
- Blanton, M. R., Lin, H., Lupton, R. H., et al. 2003b, *AJ*, 125, 2276
- Boselli, A. & Gavazzi, G. 2006, *PASP*, 118, 517
- Bower, R. G., Benson, A. J., Malbon, R., et al. 2006, *MNRAS*, 370, 645
- Budzynski, J. M., Kopolov, S. E., McCarthy, I. G., McGee, S. L., & Belokurov, V. 2012, *MNRAS*, 423, 104
- Carlberg, R. G., Yee, H. K. C., Ellingson, E., et al. 1997, *ApJ*, 476, L7
- Cavaliere, A. & Fusco-Femiano, R. 1976, *A&A*, 49, 137
- Colless, M. & Dunn, A. M. 1996, *ApJ*, 458, 435
- Cortese, L., Gavazzi, G., Boselli, A., et al. 2006, *A&A*, 453, 847
- Cox, A. N., ed. 2000, *Allen's Astrophysical Quantities* (Springer-Verlag New York, Inc.)
- de Theije, P. A. M. & Katgert, P. 1999, *A&A*, 341, 371
- Diaferio, A. 1999, *MNRAS*, 309, 610
- Diaferio, A. & Geller, M. J. 1997, *ApJ*, 481, 633
- Diaferio, A., Kauffmann, G., Balogh, M. L., et al. 2001, *MNRAS*, 323, 999
- Dickens, R. J. & Moss, C. 1976, *MNRAS*, 174, 47
- Dressler, A., Oemler, Jr., A., Poggianti, B. M., et al. 2013, *ApJ*, 770, 62
- Finn, R. A., Balogh, M. L., Zaritsky, D., Miller, C. J., & Nichol, R. C. 2008, *ApJ*, 679, 279
- Finn, R. A., Zaritsky, D., McCarthy, Jr., D. W., et al. 2005, *ApJ*, 630, 206
- Fisher, D., Fabricant, D., Franx, M., & van Dokkum, P. 1998, *ApJ*, 498, 195
- Fujita, Y. 2004, *PASJ*, 56, 29
- Gill, S. P. D., Knebe, A., & Gibson, B. K. 2005, *MNRAS*, 356, 1327
- Goto, T. 2005a, *MNRAS*, 357, 937
- Goto, T. 2005b, *MNRAS*, 359, 1415
- Gunn, J. E. & Gott, III, J. R. 1972, *ApJ*, 176, 1
- Haines, C. P., Gargiulo, A., La Barbera, F., et al. 2007, *MNRAS*, 381, 7
- Haines, C. P., Gargiulo, A., & Merluzzi, P. 2008, *MNRAS*, 385, 1201
- Haines, C. P., Pereira, M. J., Sanderson, A. J. R., et al. 2012, *ApJ*, 754, 97
- Hernández-Fernández, J. D., Iglesias-Páramo, J., & Vílchez, J. M. 2012a, *ApJS*, 199, 22
- Hernández-Fernández, J. D., Vílchez, J. M., & Iglesias-Páramo, J. 2012b, *ApJ*, 751, 54

- Hwang, H. S. & Lee, M. G. 2008, *ApJ*, 676, 218
- Iglesias-Paramo, J., Boselli, A., Cortese, L., Vilchez, J. M., & Gavazzi, G. 2002, *A&A*, 384, 383
- Kauffmann, G., Heckman, T. M., Budavári, T., et al. 2007, *ApJS*, 173, 357
- Kaviraj, S., Kirkby, L. A., Silk, J., & Sarzi, M. 2007, *MNRAS*, 382, 960
- Kennicutt, Jr., R. C. 1998, *ARA&A*, 36, 189
- Kewley, L. J., Jansen, R. A., & Geller, M. J. 2005, *PASP*, 117, 227
- Koopmann, R. A. & Kenney, J. D. P. 2004, *ApJ*, 613, 866
- Lewis, I., Balogh, M., De Propriis, R., et al. 2002, *MNRAS*, 334, 673
- Lopes, P. A. A., Ribeiro, A. L. B., & Rembold, S. B. 2013, *ArXiv e-prints*
- Mahajan, S., Mamon, G. A., & Raychaudhury, S. 2011, *MNRAS*, 416, 2882
- Mamon, G. A., Sanchis, T., Salvador-Solé, E., & Solanes, J. M. 2004, *A&A*, 414, 445
- Martin, D. C., Fanson, J., Schiminovich, D., et al. 2005, *ApJ*, 619, L1
- Martin, D. C., Small, T., Schiminovich, D., et al. 2007, *ApJS*, 173, 415
- Merluzzi, P., Mercurio, A., Haines, C. P., et al. 2010, *MNRAS*, 402, 753
- Merritt, D. 1987, *ApJ*, 313, 121
- Mohr, J. J., Geller, M. J., & Wegner, G. 1996, *AJ*, 112, 1816
- Morrissey, P., Schiminovich, D., Barlow, T. A., et al. 2005, *ApJ*, 619, L7
- Mould, J. R., Huchra, J. P., Freedman, W. L., et al. 2000, *ApJ*, 529, 786
- Navarro, J. F., Frenk, C. S., & White, S. D. M. 1997, *ApJ*, 490, 493
- Oman, K. A., Hudson, M. J., & Behroozi, P. S. 2013, *MNRAS*, 431, 2307
- Park, C. & Hwang, H. S. 2009, *ApJ*, 699, 1595
- Pimbblet, K. A. 2011, *MNRAS*, 411, 2637
- Pimbblet, K. A., Roseboom, I. G., & Doyle, M. T. 2006, *MNRAS*, 368, 651
- Poggianti, B. M., von der Linden, A., De Lucia, G., et al. 2006, *ApJ*, 642, 188
- Popesso, P., Biviano, A., Romaniello, M., & Böhringer, H. 2007, *A&A*, 461, 411
- Porter, S. C., Raychaudhury, S., Pimbblet, K. A., & Drinkwater, M. J. 2008, *MNRAS*, 388, 1152
- Ramirez, A. C. & de Souza, R. E. 1998, *ApJ*, 496, 693
- Rines, K. & Diaferio, A. 2006, *AJ*, 132, 1275
- Rines, K., Geller, M. J., Kurtz, M. J., & Diaferio, A. 2003, *AJ*, 126, 2152
- Rines, K., Geller, M. J., Kurtz, M. J., & Diaferio, A. 2005, *AJ*, 130, 1482
- Salim, S., Charlot, S., Rich, R. M., et al. 2005, *ApJ*, 619, L39
- Sato, T. & Martin, C. L. 2006, *ApJ*, 647, 946
- Serna, A. & Gerbal, D. 1996, *A&A*, 309, 65
- Serra, A. L. & Diaferio, A. 2013, *ApJ*, 768, 116
- Serra, A. L., Diaferio, A., Murante, G., & Borgani, S. 2011, *MNRAS*, 412, 800
- Sodre, Jr., L., Capelato, H. V., Steiner, J. E., & Mazure, A. 1989, *AJ*, 97, 1279
- Solanes, J. M., Manrique, A., García-Gómez, C., et al. 2001, *ApJ*, 548, 97
- Springel, V., White, S. D. M., Jenkins, A., et al. 2005, *Nature*, 435, 629
- Strauss, M. A., Weinberg, D. H., Lupton, R. H., et al. 2002, *AJ*, 124, 1810
- Treu, T., Ellis, R. S., Kneib, J., et al. 2003, *ApJ*, 591, 53
- van der Marel, R. P., Magorrian, J., Carlberg, R. G., Yee, H. K. C., & Ellingson, E. 2000, *AJ*, 119, 2038



Wojtak, R. & Łokas, E. L. 2010, MNRAS, 408,  
2442

Wolf, C., Aragón-Salamanca, A., Balogh, M.,  
et al. 2009, MNRAS, 393, 1302

Wyder, T. K., Martin, D. C., Schiminovich, D.,  
et al. 2007, ApJS, 173, 293